



Local Correlation-based Transition Models for High-Reynolds-Number Wind Turbine Airfoils

Yong Su Jung¹, Ganesh Vijayakumar², Shreyas Ananthan², and James Baeder¹

¹University of Maryland, College Park, MD

²National Renewable Energy Laboratory, Golden, CO

Correspondence: Yong Su Jung (jung9053@umd.edu)

Abstract. Modern wind-turbine airfoil design requires robust performance predictions for varying thicknesses, shapes, and appropriate Reynolds numbers. The airfoils of current large offshore wind turbines operate with chord-based Reynolds numbers in the range of 3-15 million. Turbulence transition in the airfoil boundary layer is known to play an important role in the aerodynamics of these airfoils near the design operating point. While the lack of prediction of lift stall through Reynolds-averaged Navier-Stokes (RANS) computational fluid dynamics (CFD) is well-known, airfoil design using CFD requires the accurate prediction of the glide ratio (L/D) in the linear portion of the lift polar. The prediction of the drag bucket and the glide ratio is greatly affected by the choice of the transition model in RANS-CFD of airfoils. We present the performance of two existing local correlation-based transition models—one-equation (γ) and two-equation model ($\gamma - \overline{Re_{\theta t}}$) coupled with the Spalart-Allmaras (SA) RANS turbulence model—for offshore wind-turbine airfoils operating at a high Reynolds number. We compare the predictions of the two transition models with available experimental and CFD data in the literature in the Reynolds number range of 3-15 million including the AVATAR project measurements of the DU00-W-212 airfoil. Both transition models predict a larger L/D compared to fully turbulent results at all Reynolds numbers. The two models exhibit similar behavior at Reynolds numbers around 3 million. However, at higher Reynolds numbers, the one-equation model fails to predict the natural transition behavior due to early transition onset. The two-equation transition model predicts the aerodynamic coefficients for airfoils of various thickness at higher Reynolds numbers up to 15 million more accurately compared to the one-equation model. The two-equation model also predicts the correct trends with the variation of Reynolds number comparable to the e^N transition model. However, a limitation of this model is observed at very high Reynolds numbers of around 12-15 million where the predictions are very sensitive to the inflow turbulent intensity. The combination of the ($\gamma - \overline{Re_{\theta t}}$) transition model coupled with the Spalart-Allmaras (SA) RANS turbulence model is a robust method for performance prediction of modern wind-turbine airfoils using CFD.



1 Introduction

The aerodynamic design of increasingly large rotors (Veers et al., 2019) to satisfy the world’s wind energy needs relies on robust and accurate performance predictions at all operating conditions. The airfoils of current large wind turbines operate at chord-based Reynolds numbers of 3-15 million, as shown in Fig. 1. Laminar-turbulent boundary layer transition is a complex phenomenon that affects the aerodynamics of airfoil boundary layers near the design operating point. Reynolds-averaged Navier-Stokes (RANS) modeling using computational fluid dynamics (CFD) is a common high-fidelity modeling tool used for airfoil design. Typical RANS-CFD solvers are augmented with transition models to improve accuracy of aerodynamic predictions of airfoils.

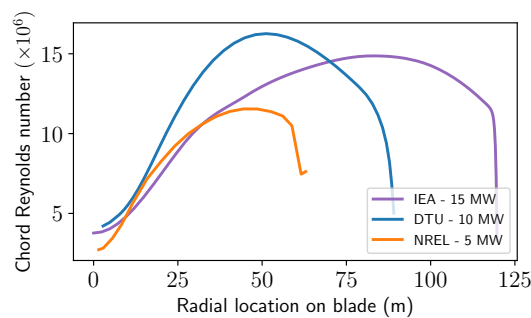


Figure 1. Variation of chord Reynolds number and airfoil thickness along the blade span for three modern commercially relevant turbines: NREL 5-MW (Jonkman et al., 2009), DTU 10-MW (Bak et al., 2013), and IEA 15-MW (Gaertner et al., 2020)

This work is part of a project to develop a machine-learning inverse-design capability for three-dimensional (3D) aerodynamic design of wind turbine rotors. In the first phase of our project, we focus on inverse-design of two-dimensional (2D) airfoils. Our goal is to develop a robust 2D airfoil capability with the appropriate transition model that can accurately predict the performance of airfoils of various thicknesses and shapes at different operating conditions to generate reliable training data for the machine-learning process. It is well-known that 2D RANS-CFD does not accurately capture the stall behavior of airfoils (Sorensen et al., 2016). However, the generation of training data for airfoil-design purposes requires the accurate prediction of the glide ratio near the design operating point of airfoils in the linear portion of the lift polar. Sorensen et al. (2016) have shown that the transition model affects the prediction of the glide ratio in this region of the lift polar along with the trends with respect to the Reynolds number.

Transition modeling and simulation are divided into analytical models based on stability theory and statistical models. The e^N model is a popular analytical transition model based on the linear stability theory. However, the application of the e^N method within a conventional RANS framework that runs on massively parallel computers is difficult because it requires solving the boundary layer equations for global flow quantities. Also, additional effort to compute N is required using either correlation with experiment (semi-empirical) or a linear stability solver (Sheng, 2017). In wind turbine applications, the e^N method has been used in either 2D RANS flow solvers or a low fidelity XFOIL code (Sorensen et al., 2016; Ceyhan et al.,



2017b). However, much more complex infrastructure is required in coupling with a full 3D RANS-CFD method. Another
45 linear stability theory-based model for coupling with the Spalart-Allmaras (SA) turbulence model is the amplification factor
transport (AFT) framework (Coder, 2019).

Statistical models like local correlation-based transition models (LCTMs) that solve prognostic transport equations for tran-
sition variables are more suitable for use with RANS-CFD models. Two major LCTMs are the two-equation $\gamma - Re_\theta$ model
developed by Langtry and Menter (2009), and the simplified one-equation γ model by Menter et al. (2015). The one-equation
50 model is preferable for wind-turbine modeling, as it satisfies Galilean invariance, a requirement for application to rotating
physical systems. These transition models were originally developed to be coupled with the shear stress transport ($k-\omega$ -SST)
turbulence model that is widely used in the wind turbine community. However, different versions of LCTM coupled to the
one-equation SA turbulence model have also been developed (Medida, 2014; Wang and Sheng, 2014; Nichols, 2019). The
SA turbulence model has advantages of robustness, reliability, and lower computational cost than the ($k-\omega$ -SST) model. The
55 LCTM-SA models have been successfully applied to a wide range of aerospace problems including rotorcraft.

Applications of RANS-CFD to wind turbine modeling have mostly focused on using the $k-\omega$ -SST turbulence model coupled
to the LCTM or the e^N -based transition model (Sorensen et al., 2016). Sorensen et al. (2014) showed that the two-equation
 $\gamma - Re_{\theta t}$ transition model fails to correctly predict natural transition behaviors at high Reynolds numbers compared to the
 e^N -based model. Two out of the four codes in the blind-test campaign (Ceyhan et al., 2017b) to predict the performance of
60 the DU00-W212 airfoil using AVATAR data (Ceyhan et al., 2017a) also used the e^N -based model. Hence, the above studies
together show the superiority of the e^N -based method over LCTM for predicting natural transition behavior for high-Reynolds-
number flows. However, there is a lack of studies using the LCTM coupled with the SA turbulence model for wind turbine
applications.

In this paper, we quantify the performance of both one-equation and two-equation LCTM coupled with the SA turbulence
65 model in simulating wind turbine airfoils at a wide range of Reynolds numbers. We compare our simulation results to not
only experiments but also the other predictions using different transition models (e.g. e^N -based). First, the formulations of
correlation-based transition models are presented briefly for completeness in Section 2. Then, we show validation results for
the turbulence and transition models at a moderate Reynolds number in Section 3. Section 4 analyzes the differences between
the predictions from the one-equation and two-equation transition models through comparison to the measurements from the
70 AVATAR project (Ceyhan et al., 2017a) on the DU00-W-212 airfoil at Reynolds numbers 3-15 million. We then compare the
predictions of the two LCTMs for airfoils from three modern, commercially relevant wind turbines, NREL 5 MW (Jonkman
et al., 2009), DTU 10 MW (Bak et al., 2013), and IEA 15 MW (Gaertner et al., 2020). Our simulation results are compared with
available reference data from experiments and/or other simulations in the literature. Finally, we conclude with a discussion of
the transition models in RANS-CFD solvers for airfoil design in modern wind turbines.



75 2 Methodology

2.1 Reynolds-Averaged Navier-Stokes Solver

The Hamiltonian solver (HAM2D) is a Reynolds-averaged Navier-Stokes (RANS) flow solver that was developed at the University of Maryland (Jung and Baeder, 2019). This is a parallel solver for the solution of the two-dimensional compressible Navier-Stokes equations on unstructured meshes using finite volume formulation. A fifth-order weighted essentially non-oscillatory (WENO) scheme is used for spatial reconstruction and Roe's approximate Riemann solver is used to compute inviscid fluxes. Viscous fluxes are calculated using second-order central differencing. For the steady-state solution, the preconditioned generalized minimum residual (GMRES) is used as implicit time-integration method. The turbulent boundary layer is modeled using one-equation SA model. Both the one-equation γ -transition model (Menter et al., 2015) and the two-equation $\gamma - \overline{Re_{\theta t}}$ -SA transition models (Medida, 2014) have been coupled with the SA turbulence model to predict boundary layer transition if necessary. In this study, the incompressible flow condition was approximated in the compressible solver using a freestream Mach number of 0.1. The Reynolds number based on chord length and angle of attack was adjusted for test flow conditions.

Our in-house automated airfoil mesh generation was used for various test airfoils, which is designed to require relatively few control inputs from airfoil coordinates (Costenoble et al., 2018). For efficient meshing, the surface point distribution (clustering/stretching) is based on local sharp corners or different surface curvatures along the airfoil. An O-type grid is used to allow for a finite-thickness trailing edge. A strand-/advancing-front-based method is used to generate a body-fitted mesh around the airfoil, and the triangle elements are used to extend the domain to the outer boundary. All triangular elements are transformed to obtain a pure quadrilateral mesh, which is required by the flow solver. In previous studies, the current flow solver and automated mesh generation have been validated through various canonical problems (Costenoble et al., 2017, 2018; Jung and Baeder, 2019). For the simulations in this paper, the number of nodes in the wrap-around direction was fixed as 400 points, as determined through a grid convergence study (Appendix A), and the initial wall-normal spacing was varied according to the test Reynolds number, such that $y^+ = 1$. The outer boundary was placed 300 chord lengths away from the airfoil where the far-field boundary condition was imposed. Figure 2 shows the mesh generated using this method around the DU21-A17 airfoil at a Reynolds number of 9×10^6 as an example. The convergence of the residuals and the aerodynamic coefficients with solver iterations is shown in Appendix B.

2.2 Two-Equation Laminar-Turbulent Boundary Layer Transition Model

The two-equation LCTM model used in this study is the $\gamma - \overline{Re_{\theta t}}$ -SA model, also known as the Medida-Baeder transition model. A brief description of this transition model is presented in this paper and a detailed description can be found in Medida (2014); Jung and Baeder (2019). This transition model can predict natural transition, separation-induced transition, and bypass transition and has been validated through various canonical problems. The transition model uses the concept of intermittency, γ , in order to trigger transition locally. The intermittency is a scalar transport variable that varies between 0 (pure laminar) and

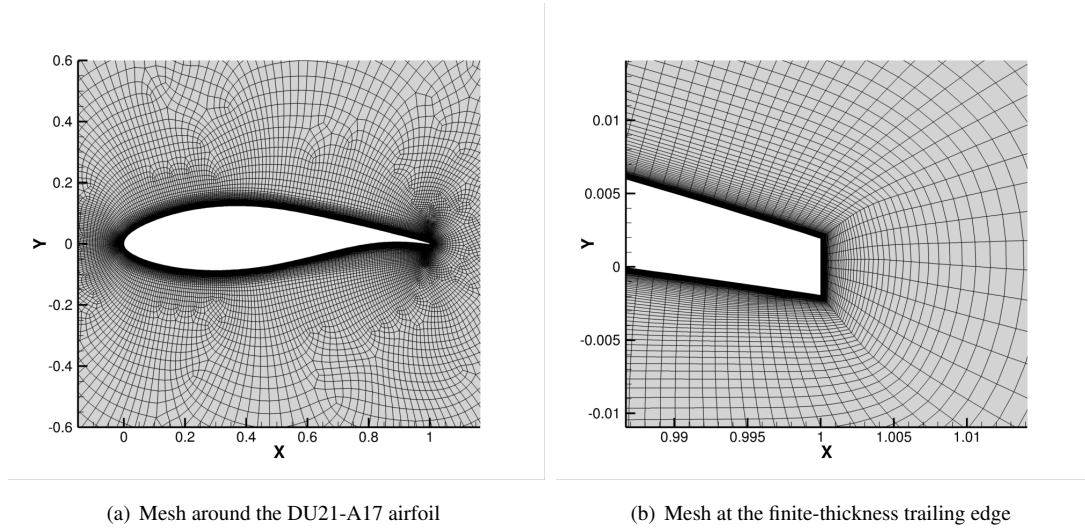


Figure 2. Example of a computational mesh for the DU21-A17 airfoil

1 (pure turbulent). The transport equation for the intermittency is given by

$$\frac{D(\rho\gamma)}{Dt} = P_\gamma - D_\gamma + \frac{\partial}{\partial x_j} \left[(\mu + \mu_t) \frac{\partial \gamma}{\partial x_j} \right], \quad (1)$$

where P_γ and D_γ denote the production and destruction term, respectively.

110 The transport equation for transition momentum thickness Reynolds number, $\overline{Re_{\theta_t}}$, is used to account for history effects of pressure gradient on determining the onset of transition. This equation is given by

$$\frac{D(\rho \overline{Re_{\theta_t}})}{Dt} = P_{\theta_t} + \frac{\partial}{\partial x_j} \left[2.0(\mu + \mu_t) \frac{\partial \overline{Re_{\theta_t}}}{\partial x_j} \right], \quad (2)$$

where $P_{\theta_t} = 0.03 \frac{\rho}{\bar{\rho}} (Re_{\theta_t} - \overline{Re_{\theta_t}})(1.0 - F_{\theta_t})$.

Once the distribution of $\overline{Re_{\theta_t}}$ in the computational domain is solved, the critical momentum thickness Reynolds number
 115 is obtained through $Re_{\theta_c} = 0.62 \cdot \overline{Re_{\theta_t}}$. Then, the intermittency production can be triggered based on the ratio of the local vorticity Reynolds number, Re_v , to the Re_{θ_c} . For the production term, the transition onset momentum thickness Reynolds number, Re_{θ_t} , is computed through the empirical correlations in an iterative manner, which are functions of the streamwise pressure gradient parameter, λ_θ , and the inflow turbulent intensity. λ_θ is defined as

$$\lambda_\theta = \frac{\rho \theta^2}{\mu} \frac{dU}{ds}, \quad (3)$$

$$120 \frac{dU}{ds} = \frac{u}{U} \frac{dU}{dx} + \frac{v}{U} \frac{dU}{du} + \frac{w}{U} \frac{dU}{dz}, \quad (4)$$

where $U = \sqrt{u^2 + v^2 + w^2}$.



When this transition model is coupled with the SA turbulence model, the intermittency is used to control only the production term of the transported variable, $\tilde{\nu}$, as

$$\frac{D\tilde{\nu}}{Dt} = \gamma P_{\tilde{\nu}} - D_{\tilde{\nu}} + \frac{1}{\sigma} [\nabla \cdot ((\nu + \tilde{\nu})\nabla\tilde{\nu}) + c_{b2}(\nabla\tilde{\nu})^2]. \quad (5)$$

125 There are two major differences in the current implementation of the transition model compared to the $\gamma - Re_{\theta}$ model by Langtry and Menter (2009); the first is the omission of separation-induced transition modification, γ_{sep} , which is not required in this model, and the second is the use of a nonlocal variable, G_{onset} , in both P_{γ} and D_{γ} .

2.3 One-Equation Laminar-Turbulent Boundary Layer Transition Model

130 The one-equation transition model first proposed by Menter et al. (2015) uses only the intermittency variable, γ ; hence, only the transport equation for the intermittency is required as shown in Eq 1. Both production and destruction terms for the intermittency are different compared to the two-equation model. The transport equation for $\overline{Re_{\theta t}}$ is replaced with the empirical-based formulation as follows for obtaining $Re_{\theta c}$.

$$Re_{\theta c}(Tu_L, \lambda_{\theta L}) = C_{TU1} + C_{TU2} \exp[-C_{TU3} Tu_L F_{PG}]. \quad (6)$$

135 Our implementation of the one-equation model uses modified coefficients of C_{TU1} , C_{TU2} , and C_{TU3} compared to that by Menter et al. (2015), which gives better correlation with the experiments than the original values, as shown by Colonia et al. (2016). The modified values of the constants are

$$C_{TU1} = 163.0, C_{TU2} = 1002.25, C_{TU3} = 1.0. \quad (7)$$

140 In the $Re_{\theta c}$ formulation, F_{PG} is introduced to sensitize the transition onset to the streamwise pressure gradient. The pressure gradient parameter, λ_{θ} , in Eq. 4 is approximated as $\lambda_{\theta L}$ in the model; thus it becomes only a function of wall normal direction velocity and coordinate in addition to the kinematic viscosity, ν .

$$\lambda_{\theta L} = -7.57 \cdot 10^{-3} \frac{dV}{dy} \frac{d_w^2}{\nu} + 0.0128, \quad (8)$$

$$\lambda_{\theta L} = \min(\max(\lambda_{\theta L}, -1.0), 1.0), \quad (9)$$

$$\frac{dV}{dy} = \Delta(\mathbf{n} \cdot \mathbf{V}) \cdot \mathbf{n}, \quad (10)$$

where d_w is the wall distance.

145 The one-equation transition model was coupled with the SA turbulence model first by Nichols (2019) using the equations as follows:



$$\frac{D\tilde{\nu}}{Dt} = \tilde{P}_{\tilde{\nu}} + P_{\tilde{\nu}}^{lim} - \tilde{D}_{\tilde{\nu}} + \frac{1}{\sigma} [\nabla \cdot ((\nu + \tilde{\nu})\nabla\tilde{\nu}) + c_{b2}(\nabla\tilde{\nu})^2], \quad (11)$$

$$\tilde{P}_{\tilde{\nu}} = \gamma_s P_{\tilde{\nu}}, \quad (12)$$

$$\tilde{D}_{\tilde{\nu}} = \max(\gamma_s, 0.1) D_{\tilde{\nu}}. \quad (13)$$

150 It should be noted that the intermittency is used to control both the production and destruction terms of the SA model unlike the two-equation transition model. Nichols (2019) also defined a re-scaled transition variable, γ_s , which goes from zero at the wall to one in turbulent regions of the flow as below. This is because the SA model requires the production source term to go to zero in laminar regions of the flow.

$$\gamma_s = \frac{\min(\gamma, 1) - 1/c_{e2}}{1 - 1/c_{e2}}, \quad (14)$$

155 $\gamma_s = \max[\min(\gamma_s, 1), 0]. \quad (15)$

In addition, $P_{\tilde{\nu}}^{lim}$ as an additional production term was proposed to ensure the generation of turbulent kinetic energy at the transition point for low free-stream turbulence intensity levels. Finally, for the local turbulence intensity computation, Tu_L , turbulent kinetic energy, k , and specific dissipation, ω , variables were replaced as shown in the equations below because these variables are not available in the SA turbulence model.

160 $Tu_L = \min\left(100 \frac{\sqrt{2k/3}}{\omega d_w}\right), \quad (16)$

$$\omega = S/0.3, \quad (17)$$

$$k = \frac{\mu_t \omega}{\rho}. \quad (18)$$

where S is the strain rate magnitude.

165 However, the current study employs a measured turbulence intensity from an experiment and assumes a constant turbulence intensity in the entire flow field. The assumption of the constant turbulence intensity in the flow field is valid for external aerodynamic flows and has been extensively validated by previous studies for both the two-equation transition model (Medida, 2014; Jung and Baeder, 2019) and the one-equation transition model (Lee and Baeder, 2021). Recently, Lee and Baeder (2021) validated the current version of the one-equation LCTM coupled with the SA turbulence model through canonical problems in both two and three dimensions, and we use the same formulation for the simulations in this paper.



170 3 Validation

In this section, we show code-to-code comparisons and validation studies for the SA turbulence model and the transition models using our solver HAM2D. First, we compare the performance of the SA turbulence model without any transition model against that of other codes for reference cases. Then, we show code-to-code comparison and validation of both transition models against experimental data for the S809 airfoil at a moderate Reynolds number.

175 The performance of the SA turbulence model using the current solver and mesh-generation approach has been validated in previous studies (Jung et al., 2017; Jung and Baeder, 2019; Jung, 2019) through various test cases from NASA Turbulence Modeling Resource (TMR, 2017). The test cases include a 2D zero pressure gradient flat plate, 2D bump-in-channel, and NACA 0012 airfoil. The case of turbulent flow past a NACA0012 airfoil is shown in this paper as an example. The flow condition is a free-stream Mach number of 0.15, a Reynolds number of 6 million, and three angles of attack (0, 10, 15°). A
 180 structured airfoil C-type mesh (897 × 257) provided by the TMR website is used for the current simulation. Table 1 shows the comparison of the lift and drag coefficients of the NACA0012 airfoil using the SA turbulence model. The force coefficients predicted by HAM2D are comparable to the results predicted by well-established legacy codes.

Table 1. Comparison of lift and drag coefficient for the NACA0012 airfoil using the SA turbulence model against other implementations in NASA-TMR (TMR, 2017).

Codes	C_l ($\alpha = 0^\circ$)	C_l ($\alpha = 10^\circ$)	C_l ($\alpha = 15^\circ$)	C_d ($\alpha = 0^\circ$)	C_d ($\alpha = 10^\circ$)	C_d ($\alpha = 15^\circ$)
CFL3D	approx 0	1.0909	1.5461	0.00819	0.01231	0.02124
FUN3D	approx 0	1.0983	1.5547	0.00812	0.01242	0.02159
TURN3	approx 0	1.1000	1.5642	0.00830	0.01230	0.02140
mStrand	approx 0	1.0967	1.5621	0.00804	0.01251	0.02195
HAM2D	approx 0	1.0907	1.5459	0.00812	0.01232	0.02127

For wind-turbine airfoils, we compare our predictions using the SA model with those from EllipSys2D for FFA-301 and FFA-360GF airfoils (Bak et al., 2013) using the $k-\omega$ -SST model at a Reynolds number of 10 million under a fully turbulent
 185 flow assumption. FFA-360GF is a very thick airfoil with $t/c_{\max} = 36\%$ and a gurney flap. Figure 3 compares the lift coefficient, drag coefficient, and lift-to-drag ratio as a function of angle of attack from each simulation. Both predictions show very good agreement in the drag coefficient and lift-to-drag ratio over the test angles of attack from -4° to 20° . Also, the linear portion of the lift polar is well matched between the predictions. This shows that the one-equation SA model provides similar performance compared to the two-equation $k-\omega$ -SST model under fully turbulent flow conditions. This implementation of the SA model will
 190 be coupled with transition models for free-transition flow simulations in this paper.

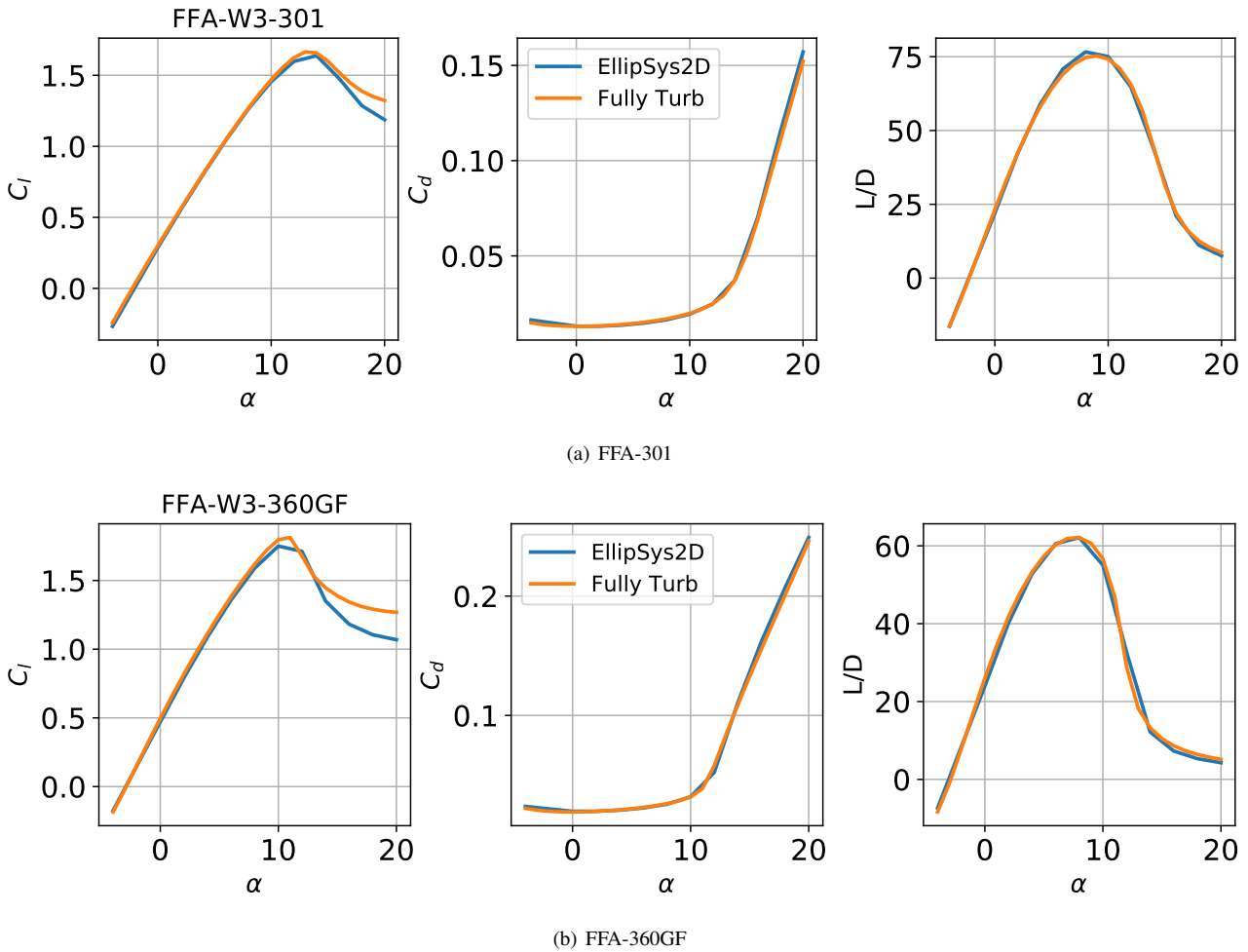


Figure 3. Comparison of aerodynamic performance predicted by HAM2D using the SA turbulence model with that from EllipSys2D using the $k-\omega$ -SST turbulence model (Bak et al., 2013) under fully turbulent flow assumptions at a Reynolds number of 10 million.

The two transition models considered in this study are evaluated through the S809 airfoil used in the NREL Phase VI wind turbine (Hand et al., 2001). We show validation by the aerodynamic performance prediction against experimental data (Somers, 1997) as well as simulation results using NASA’s OVERFLOW code using the SA-neg turbulence model (Allmaras et al., 2012), SA-neg turbulence model with AFT2019 transition model (Coder, 2019). We also compare our results with those from the 2018 transition modeling workshop by Hall (2018) using the two-equation transition model in OVERFLOW. The test flow condition is at free-stream and the two-equation Mach number of 0.1, Reynolds number of 2 million based on chord length, and a free-stream turbulence intensity of 0.05%. We use the medium-resolution reference structured C-grid from the 2018 transition modeling workshop (Hall, 2018) with dimensions of 705×87 including 513 points on the surface and 97 points in the wake.



200 An angle-of-attack sweep was conducted from -8° to 15° . Figure 4 compares the lift polar, drag polar, and the transition
location of the predictions from the fully-turbulent and free-transition simulations using both transition models against experi-
mental data and simulation results from Coder (2019); Hall (2018). Figure 4 (a) shows that the lift predictions from HAM2D
are slightly overpredicted in the transition simulations and underpredicted in the fully turbulent simulations compared to the
untripped experimental data while showing an identical trend with simulation results from Coder (2019). All CFD predictions
205 significantly overpredict the maximum lift coefficient due to the known limitations of 2D CFD-RANS.

Fig. 4 (b) shows that the drag predictions from HAM2D using the fully turbulent approximation are in excellent agreement
with the simulation results from Coder (2019) over the full range of angle of attack while showing a slight underprediction
in the drag bucket compared to the tripped boundary layer experimental data. The HAM2D predictions using both transition
models show a similar underprediction inside the drag bucket while having excellent agreement with results from the AFT2019
210 model (Coder, 2019). The two-equation transition model predicts a slightly lower drag than the one-equation model inside the
drag bucket and also shows an earlier departure from the drag bucket near a lift coefficient of 0.6 similar to the results using
two-equation model from Hall (2018).

Figure 4 (c) compares the transition onset location, X_T , predicted by the current transition models with experimental data
on both the upper and lower sides of the airfoil. The transition onset location was determined by picking up the point in the
215 middle of a sharp increase in the intermittency on the surface. As the angle of attack increases, the transition point on the upper
surface moves to the stagnation point due to an increasing adverse pressure gradient. On the other hand, the transition onset
on the lower surface moves downstream due to an increasing favorable pressure gradient with an increasing angle of attack.
The transition occurs due to a short and intense laminar separation bubble on both sides of the airfoil (separation-induced
transition). Overall, the transition onset locations predicted by both transition models match well with the experimental data.
220 The sharp movement on the upper surface at the 6° angle of attack was well captured by the two-equation model. However,
this movement was predicted at 8° from the one equation model. This difference in the onset locations explains the earlier
departure from the drag bucket using the two-equation model compared to the one-equation or the AFT2019 model.

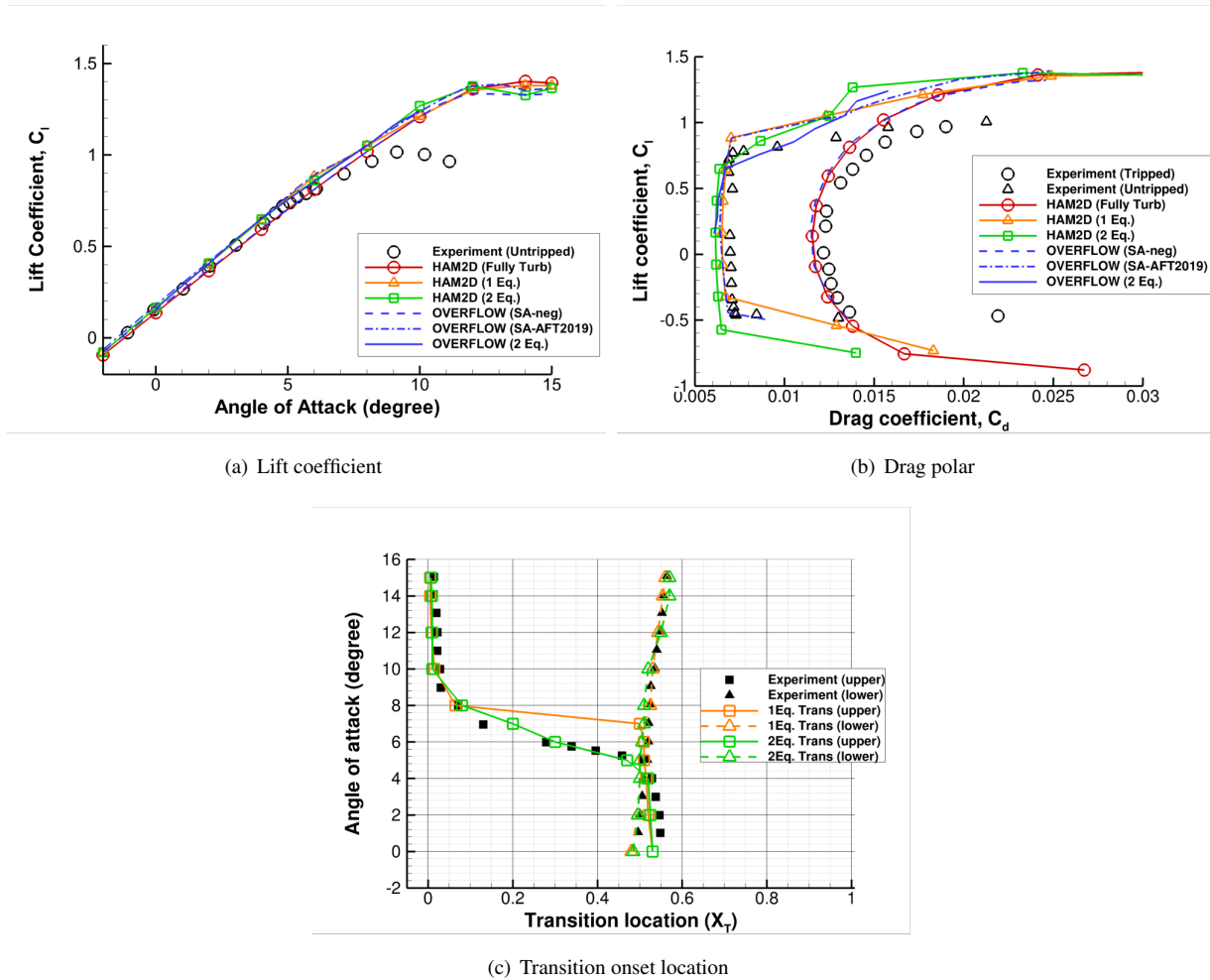


Figure 4. Comparison of (a) lift polar, (b) drag polar, and (c) transition onset location for the S809 airfoil at $Re = 2 \times 10^6$ predicted by HAM2D using a fully turbulent flow approximation and one-equation and two-equation transition models with experimental data (Somers, 1997). Also shown are predictions using the NASA-OVERFLOW solver using the SA-neg turbulence model (Allmaras et al., 2012), AFT2019 transition model (Coder, 2019), and the two-equation transition model (Hall, 2018).



4 Results

We compare the aerodynamic load predictions from the one-equation and two-equation transition models on airfoils from modern wind turbines with available reference data from experiments and/or other simulation results in the literature. First, we consider the DU00-W-212 airfoil for which wind tunnel measurements are available through the AVATAR project (Ceyhan et al., 2017a) at Reynolds numbers of 3-15 million. We analyze the effect of the choice of transition model on the prediction of the transition onset location and its sensitivity to the freestream turbulent intensity. Next, we evaluate the effect of the transition model on other airfoils from three modern, commercially relevant wind turbines, NREL 5 MW (Jonkman et al., 2009), DTU 10 MW (Bak et al., 2013), and IEA 15 MW (Gaertner et al., 2020).

4.1 DU00-W-212 airfoil - AVATAR

The AVATAR project from the European Union focused on aerodynamics of large rotors (AVA, 2018). The aerodynamic measurements on the DU00-W-212 airfoil from wind-tunnel experiments at conditions similar to those of 10 MW+ turbines were made publicly available through this project (Ceyhan et al., 2017a). We compare the effect of the one-equation and two-equation transition models against this data set as well as the results from the blind-test study by Ceyhan et al. (2017b) at Reynolds numbers of 3, 6, 9, 12, and 15 million. We also study the sensitivity of the airload predictions to the inflow turbulence intensity level through three different intensities shown in Table 2 and as performed by Ceyhan et al. (2017b).

Table 2. Test matrix to analyze the effect of transition model at different Reynolds numbers and free-stream turbulence intensities (Ti) through comparison against experimental data for the DU00-W-212 airfoil from the AVATAR project (Ceyhan et al., 2017a). Three turbulence intensities ($Ti1$, $Ti2$, $Ti3$) are tested at each Reynolds number.

	$Re=3 \times 10^6$	$Re=6 \times 10^6$	$Re=9 \times 10^6$	$Re=12 \times 10^6$	$Re=15 \times 10^6$
$Ti[\%]$	$Ti1=0.5129$ $Ti2=0.3200$ $Ti3=0.0864$	$Ti1=0.8058$ $Ti2=0.4600$ $Ti3=0.1988$	$Ti1=1.1877$ $Ti2=0.4500$ $Ti3=0.2448$	$Ti1=2.2790$ $Ti2=0.5100$ $Ti3=0.3015$	$Ti1=2.3944$ $Ti2=0.5500$ $Ti3=0.3346$

The computational grid for the DU00-W-212 airfoil was generated using the automated mesh generation procedure described in Section 2. It has 500 points in the wrap-around direction and the initial wall-normal spacing of 1.8×10^{-6} chord ($y^+=1$), which results in a grid with a resolution comparable to the meshes used by Ceyhan et al. (2017b).

We performed fully-turbulent and free-transition flow simulations with both transition models at the five different Reynolds numbers in Table 2 and the angles of attack ranging from -4° to 20° . Figure 5 shows the comparison of the lift-to-drag ratio and drag polar between the fully turbulent flow simulation results from HAM2D with the experimental data with the tripped boundary layer (Pires et al., 2016). Figure 5 (a) shows that HAM2D overpredicts the maximum lift-to-drag ratio, but the overall trend from the experiment is captured well: the slope in the linear region increases as the Reynolds number increases and the maximum lift-to-drag ratio increases as the Reynolds number increases. In Fig. 5 (b), the minimum drag coefficients match



well with experimental data in the linear region of the lift polar at all Reynolds numbers and decreases as the Reynolds number increases.

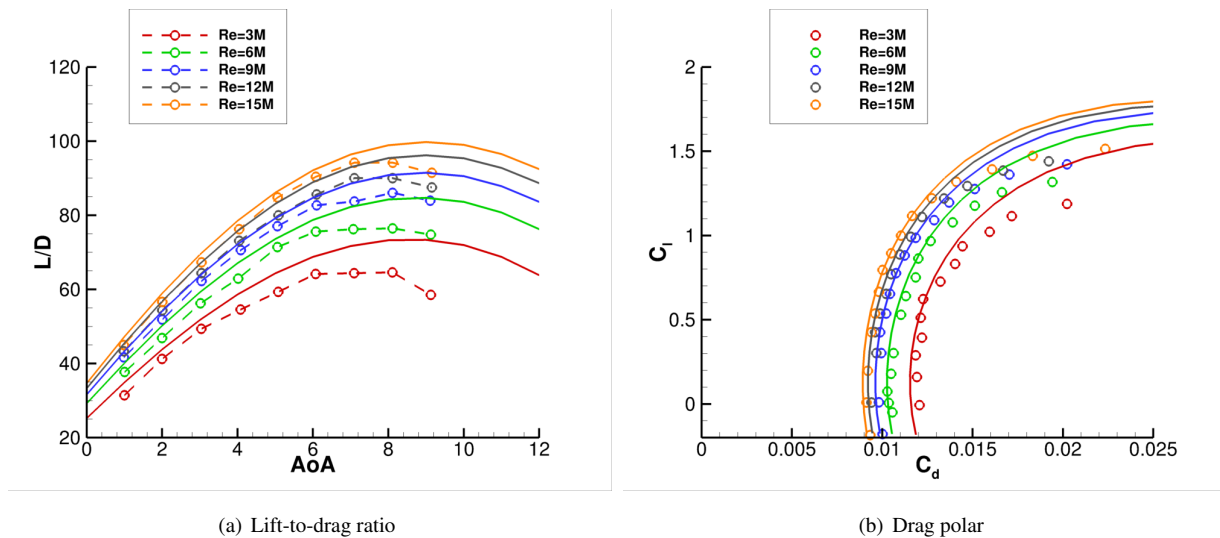


Figure 5. Comparison of (a) lift-to-drag ratio and (b) drag polar predicted by HAM2D using fully turbulent flow approximation for the DU00-W-212 airfoil against experimental data from Pires et al. (2016) with a tripped boundary layer.

Figure 6 compares the lift-to-drag (glide) ratio predicted by HAM2D using the one-equation and two-equation transition models with experimental data for the untripped boundary layer (Ceyhan et al., 2017a) and the other simulations from Pires et al. (2016). The other simulation results were obtained using the $k-\omega$ -SST turbulence model coupled with different transition models: semi-empirical e^N method by Drela-Giles for DTU-Ellipsis, e^N method combined with linear stability solver for Kiel-TAU, and Granville/Schlichting model (Yilmaz, 2017) NTUA-MapFlow. The lowest turbulence intensity level (Ti3) was used at each Reynolds number for all the computations, as shown in Table 2. The one-equation transition model in HAM2D was able to capture a reasonable maximum lift-to-drag ratio only at $Re = 3 \times 10^6$; the prediction becomes progressively worse compared to experimental data and all other simulation results at higher Reynolds numbers. On the other hand, the two-equation transition model in HAM2D shows fairly good agreement compared to both experiment and other simulation results upto $Re = 9 \times 10^6$. The prediction of the linear slope and the maximum L/D value are comparable with those of the e^N -based transition models from Pires et al. (2016). At $Re = 12 \times 10^6$ and $Re = 15 \times 10^6$, the two-equation model in HAM2D predicts a lower linear slope than all the reference results and the angle of attack for the maximum L/D is delayed. However, the results from two-equation model are much more in agreement with all reference data in Fig. 6 than the one-equation model over the entire range of Reynolds numbers.

To find the reason for underprediction of the lift-to-drag ratio using both transition models, we compare the drag polars from HAM2D predictions and the reference results in Fig. 7. At $Re = 3 \times 10^6$, the HAM2D results using both transition models predict the laminar drag bucket well. As the Reynolds number increases above 3×10^6 , the one-equation model consistently

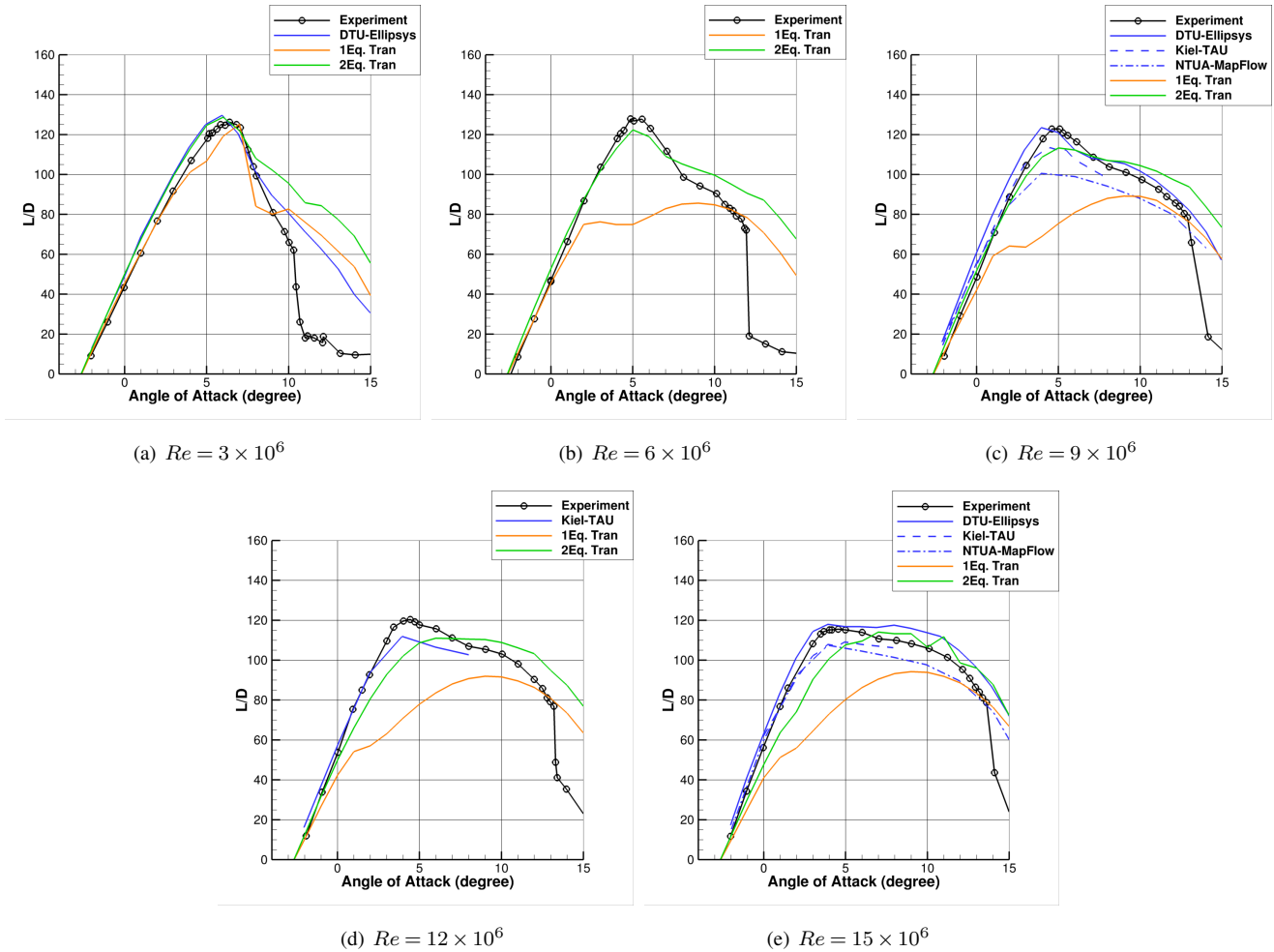


Figure 6. Comparison of the lift-to-drag ratio predicted by HAM2D using the one-equation and the two-equation transition models for the DU00-W-212 airfoil against experimental data from Ceyhan et al. (2017a). Simulation results using various transition models from DTU, Kiel, and NTUA (Pires et al., 2016) are also shown. All simulations are performed at a free-stream turbulent intensity corresponding to T13 from Table 2.

overpredicts the minimum drag while the range of angle of attack of the drag bucket becomes much smaller than the reference data. This explains the significant underprediction in lift-to-drag ratio at higher Reynolds numbers by the one-equation model. On the other hand, the two-equation model reasonably predicts the experimental drag values upto $Re = 9 \times 10^6$ compared to the other simulation results. At $Re = 12 \times 10^6$, the minimum drag is overpredicted by 6 drag counts, and the sharp corner of the laminar bucket is not properly captured. More deviation is observed at $Re = 15 \times 10^6$. However, the two-equation model in HAM2D better captures minimum drag and the sharp laminar drag bucket at higher Reynolds numbers by reducing the inflow turbulence intensity (see Fig. 9).

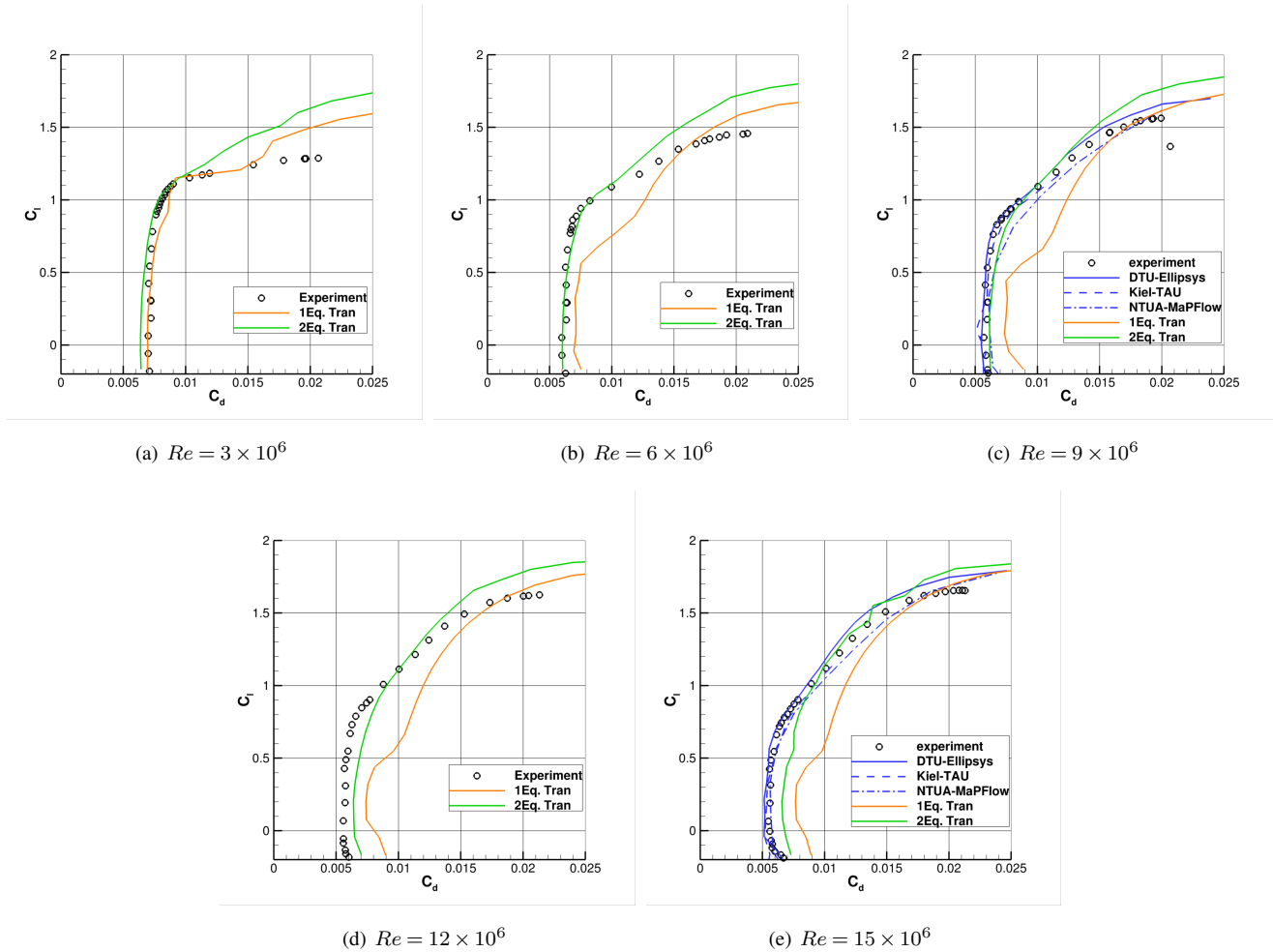


Figure 7. Comparison of drag polar predicted by HAM2D using the one-equation and the two-equation transition models for the DU00-W-212 airfoil against experimental data from Ceyhan et al. (2017a). Simulation results using various transition models from DTU, Kiel, and NTUA (Pires et al., 2016) are also shown. All simulations are performed at a free-stream turbulent intensity corresponding to Ti3 from Table 2.

Figure 8 compares the transition onset location, X_T , predicted by HAM2D using both transition models on upper and lower sides of the airfoil at two representative Reynolds numbers: 3×10^6 and 9×10^6 . These predictions are also compared with those from Ellipsys-2D using the $k-\omega$ -SST turbulence model (Sorensen et al., 2014) and different transition models: two-equation $\gamma - Re_{\theta t}$ LCTM, e^N model, and the e^N -BP model with bypass transition. At $Re = 3 \times 10^6$, the predicted transition onset locations from HAM2D using both transition models compare well with results from Ellipsys-2D, as shown in Fig. 8 (a) and (b). As the angle of attack increases, the onset location moves due to the changes in the streamwise pressure gradient similar to the behavior in the S809 airfoil in Fig. 4.



280 However, at $Re = 9 \times 10^6$, larger deviations start to occur between the predictions from the one-equation and two-equation model on both upper and lower surfaces, as shown in Fig. 8 (c) and (d). Using the one-equation model, the onset prediction rapidly moves to the stagnation point at the 2° angle of attack on the upper surface while showing erratic behavior on the lower surface. This explains the early escape of the laminar drag bucket and significant overprediction in drag by the one-equation model compared to the experimental data. Similarly, the larger deviations are also observed among the EllipSys predictions
285 (Sorensen et al., 2014) at $Re = 9 \times 10^6$. The LCTM model predicts the onset earlier than e^N and e^N -BP models on both upper and lower surfaces. It is also observed that the bypass transition starts playing a role over the natural transition at this higher Reynolds number by showing the earlier onset prediction using the e^N -BP model instead of the e^N model. The two-equation model predictions show a consistent trend in the movement of the onset location, and the results are quite similar to the results from the e^N -BP transition model on both surfaces.

290 Finally, the effect of different inflow turbulence intensity on the predictions from the two-equation transition model is shown in Fig. 9 at two different Reynolds numbers of 3×10^6 and 12×10^6 . The predicted airloads are compared from the three different turbulent intensity levels from Ti1 to Ti3, as shown in Table 2. The prediction of the lift-to-drag ratio is highly sensitive to that of the transition onset location. Both quantities are strongly dependent on the turbulent intensity level. The sensitivity of the lift-to-drag ratio on the turbulence intensity becomes stronger with an increasing Reynolds number as observed in a previous
295 study using the e^N transition model (Ceyhan et al., 2017b).

4.2 DU series airfoils and NACA64-A17

The predictions of HAM2D using both transition models for the airfoils in the NREL 5 MW turbine (Jonkman et al., 2009) are compared against experimental data available from the Delft University of Technology (DU) wind tunnel at Reynolds numbers of 6 and 7 million. The automated grid generation for these airfoils uses 400 points in the wrap-around direction based on
300 the grid-refinement study shown in Appendix A. The free-stream turbulence intensity is set to 0.1%. Figures 10 (a)-(d) show the comparison of fully turbulent and free-transition results at $Re = 7 \times 10^6$ for DU airfoils with different thickness against experimental data (Jonkman et al., 2009). A similar comparison for the NACA64-A17 airfoil at $Re = 6 \times 10^6$ is shown in Fig. 10 (e).

All simulation results, both using the fully turbulent and transition models, show similar behavior and predict the lift coefficient well in the linear region including the lift-curve slope and the zero-lift angle of attack. All simulations miss the prediction
305 of stall angle as is typical of the challenges in 2D RANS-CFD modeling of airfoils. By using either the one- or two-equation transition model, lower drag coefficients were predicted at around 0° as a result of laminar boundary layer detection. This results in a better agreement in lift-to-drag ratio against experimental data compared to the fully turbulent simulations. The prediction of the maximum lift-to-drag ratio is significantly improved using the two-equation model compared to the one-
310 equation model for all the airfoils. The one-equation model underpredicts the lift-to-drag ratio in the linear portion of the lift curve due to early transition onset as the angle of attack increases. The difference between the predictions of the maximum L/D from the one-equation and two-equation models increases for airfoils with larger maximum relative thickness $(t/c)_{\max}$. Thus, the two-equation transition model is an appropriate choice for wind-turbine airfoil simulations at high Reynolds numbers.

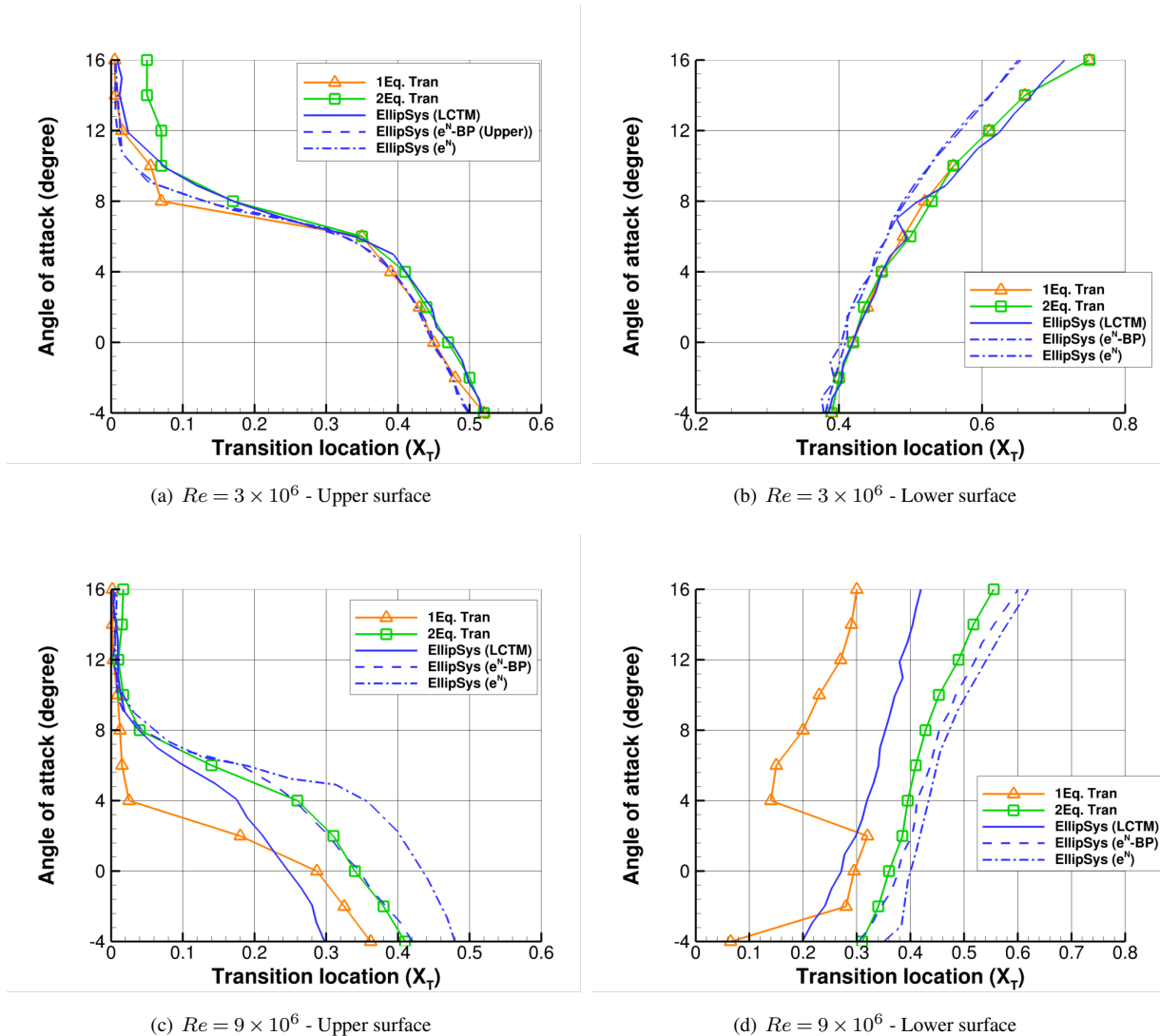


Figure 8. Comparison of variation of transition onset location with angle of attack for the DU-00-W212 airfoil predicted by HAM2D using one-equation and two-equation transition model with that by Ellipsys-2D using different transition models (Sorensen et al., 2014): LCTM - two-equation $\gamma - Re_{\theta}$ transition model, e^N model, and e^N -BP model with bypass transition.

4.3 FFA series airfoils

315 We compare the predictions of HAM2D using both transition models for the FFA-W3 series of airfoils in the DTU 10 MW (Bak et al., 2013) and the IEA 15 MW turbine (Gaertner et al., 2020) at a Reynolds number of 10 million. We also compare our results against the publicly available simulation data from Ellipsys-2D for these airfoils (Gaertner et al., 2020) using the $k-\omega$ -SST turbulence model with the semi-empirical e^N method (Drela and Giles, 1987). However, only a combination of 70%

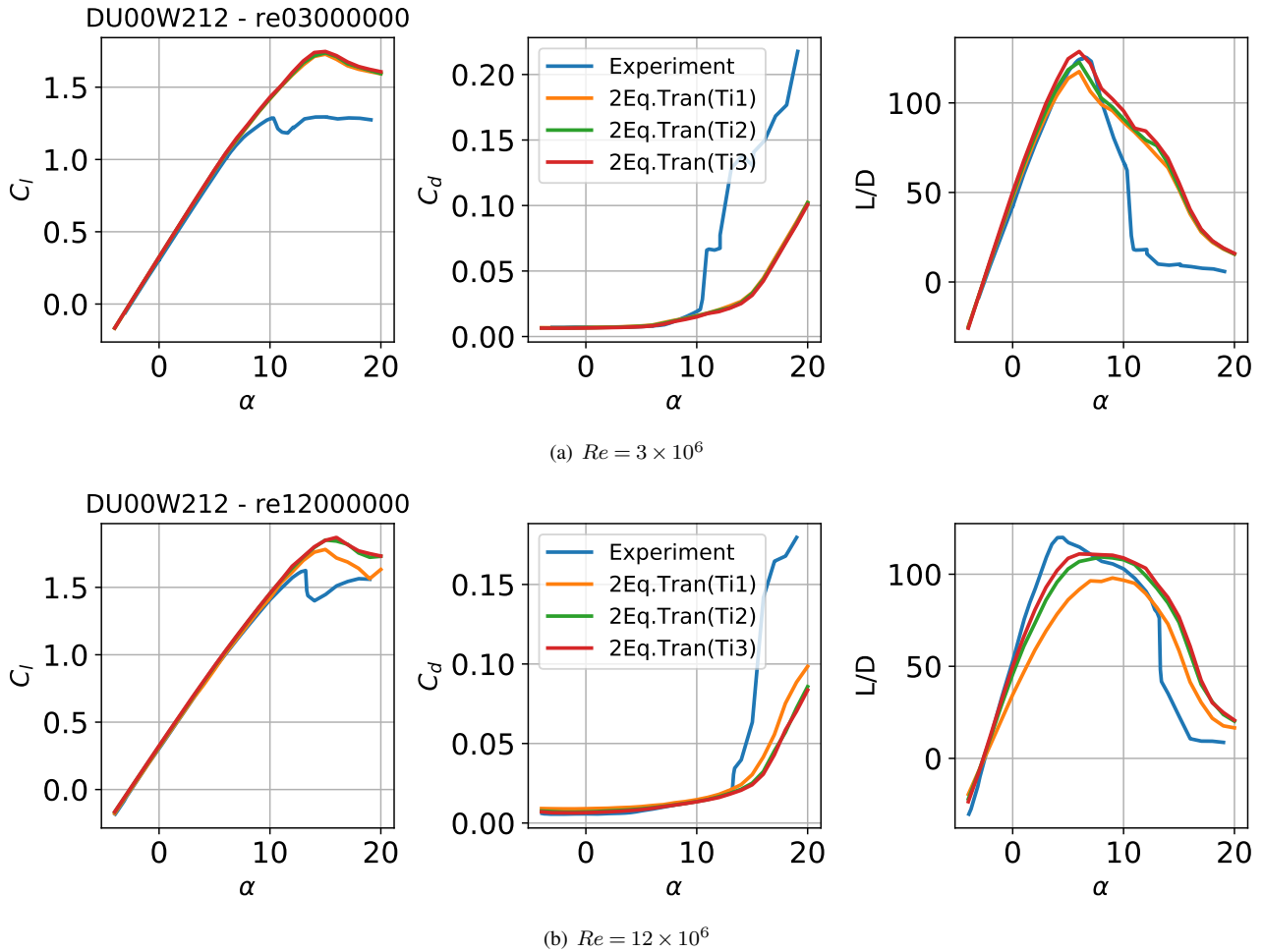
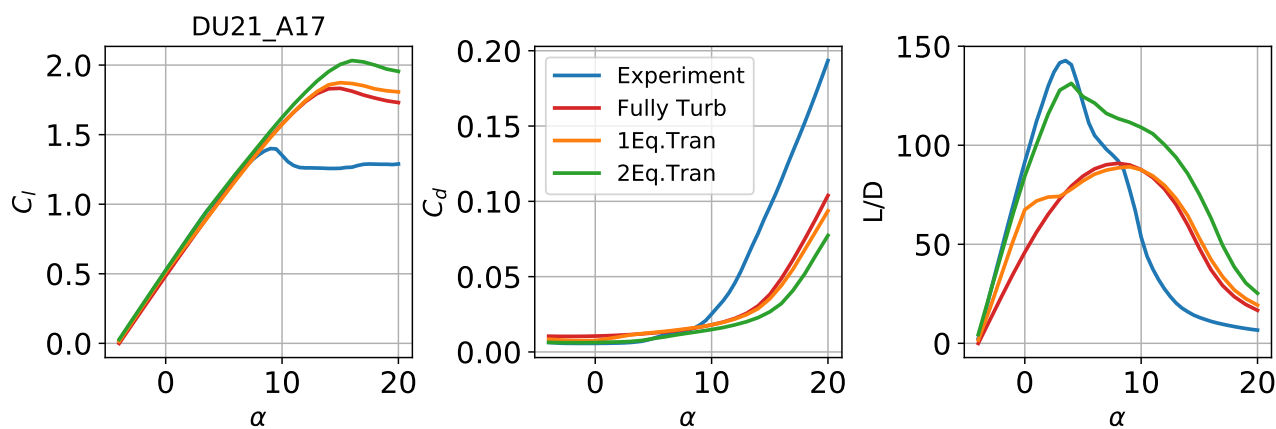


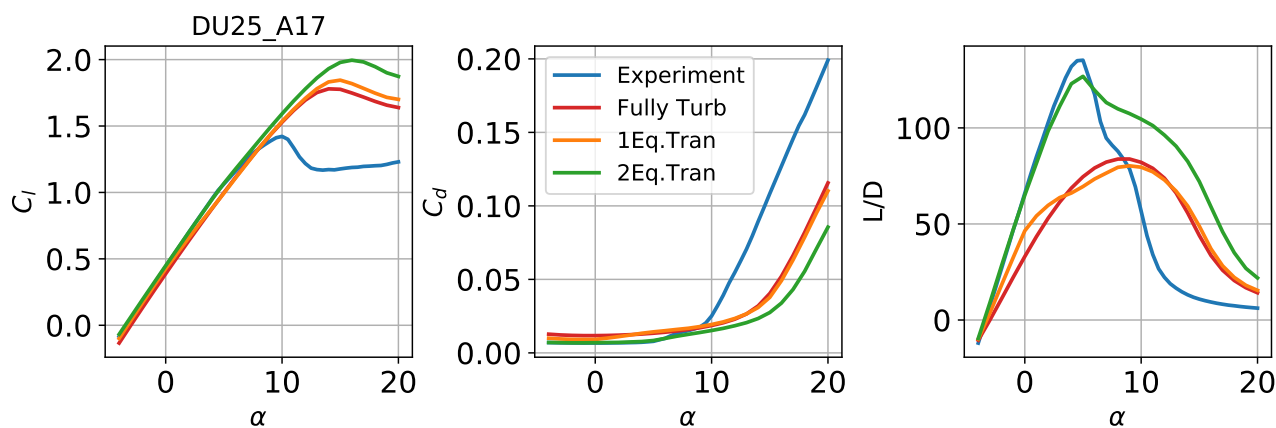
Figure 9. Sensitivity of the predictions from HAM2D using the two-equation transition model to the free-stream turbulence intensity (Ti1, Ti2, Ti3) at two Reynolds numbers $Re = 3, 12 \times 10^6$, as defined in Table 2.

free-transition/30% fully turbulently polar is available for these airfoils. Therefore, we generate the same mixed polars in this study by using one-equation and two-equation transition model for appropriate data comparison. The automated grid generation for these airfoils uses 400 points in the wrap-around direction based on the grid-refinement study shown in appendix A. The free-stream turbulence intensity is set to 0.1%.

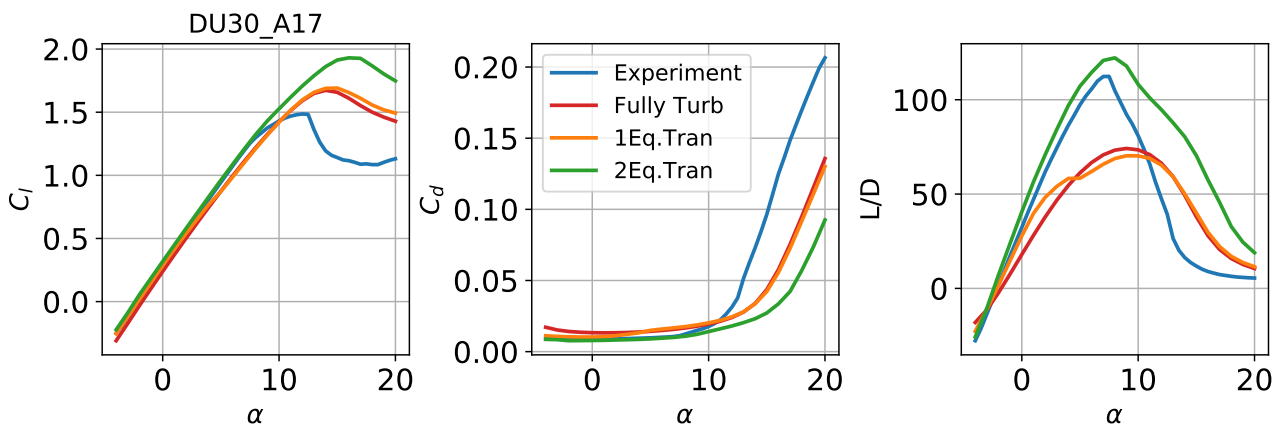
For the FFA-W3 airfoils with different airfoil thickness, our simulation results using both transition models are compared with simulation results from Ellipsys-2D (Gaertner et al., 2020) using the semi-empirical e^N method, as shown in Fig. 11. The predictions using HAM2D with the two-equation model show excellent agreement with the reference except in the case of the very thick FFA-W3-360 airfoil. The one-equation model underpredicts the lift-to-drag ratio in the linear portion of the lift curve due to early transition onset similar to the behavior seen in the DU00-W-212 (Sec. 4.1) and the NREL 5 MW airfoils



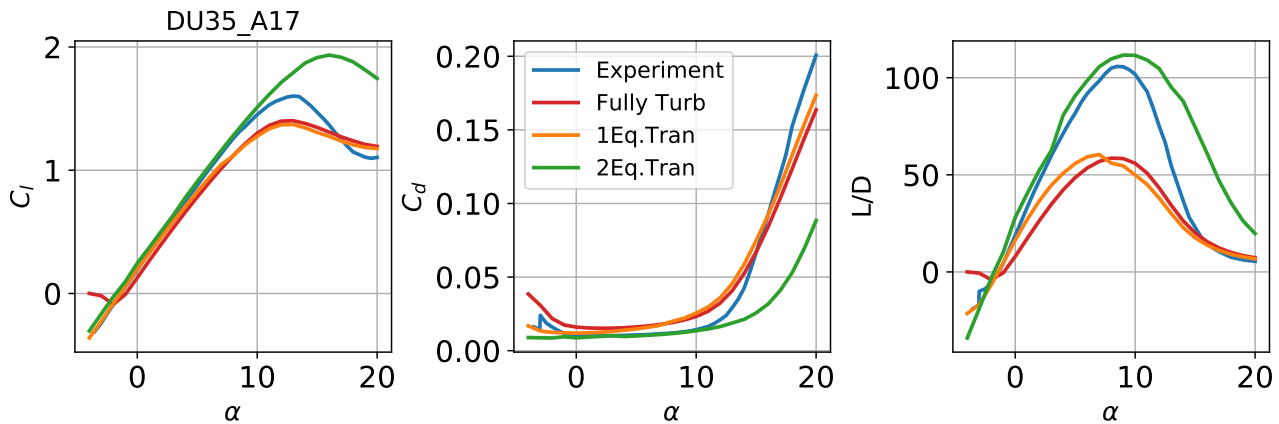
(a) DU21-A17 airfoil at $Re = 7 \times 10^6$



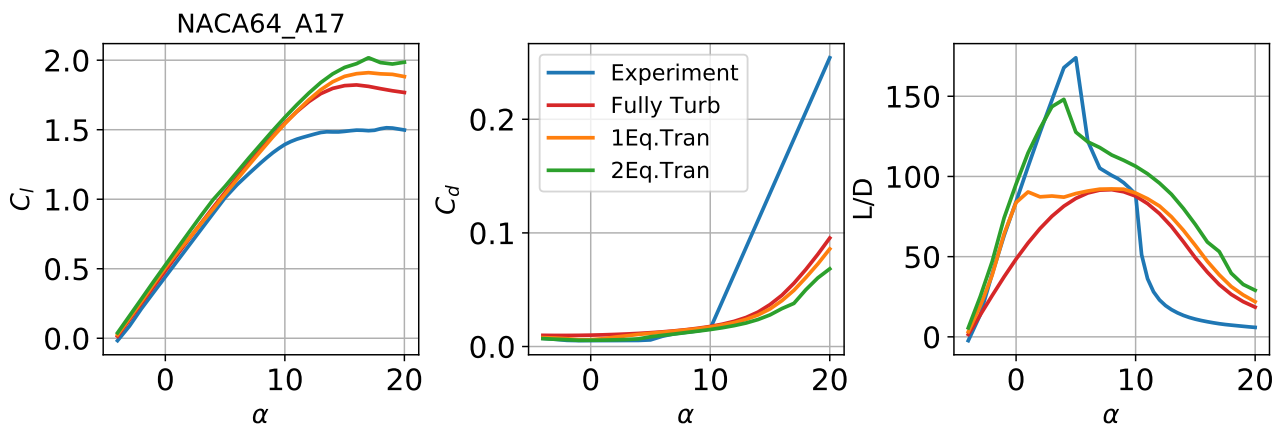
(b) DU25-A17 airfoil at $Re = 7 \times 10^6$



(c) DU30-A17 airfoil at $Re = 7 \times 10^6$



(d) DU35-A17 airfoil at $Re = 7 \times 10^6$



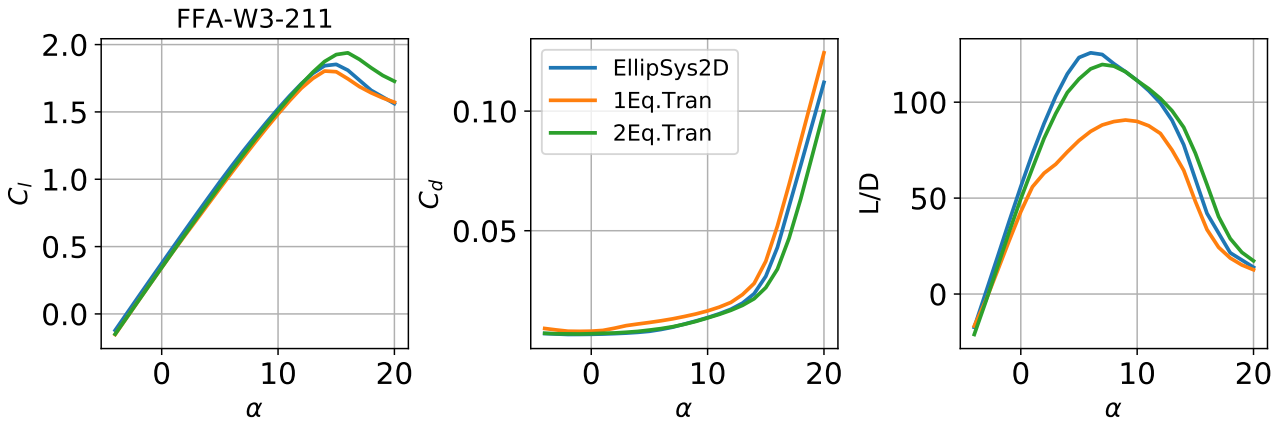
(e) NACA64-A17 airfoil at $Re = 6 \times 10^6$

Figure 10. Aerodynamic coefficient polars for DU airfoil series and NACA64-A17 using fully turbulent and free transition at $Re = 7 \times 10^6, 6 \times 10^6$ generated using HAM2D compared against experimental data (Jonkman et al., 2009).

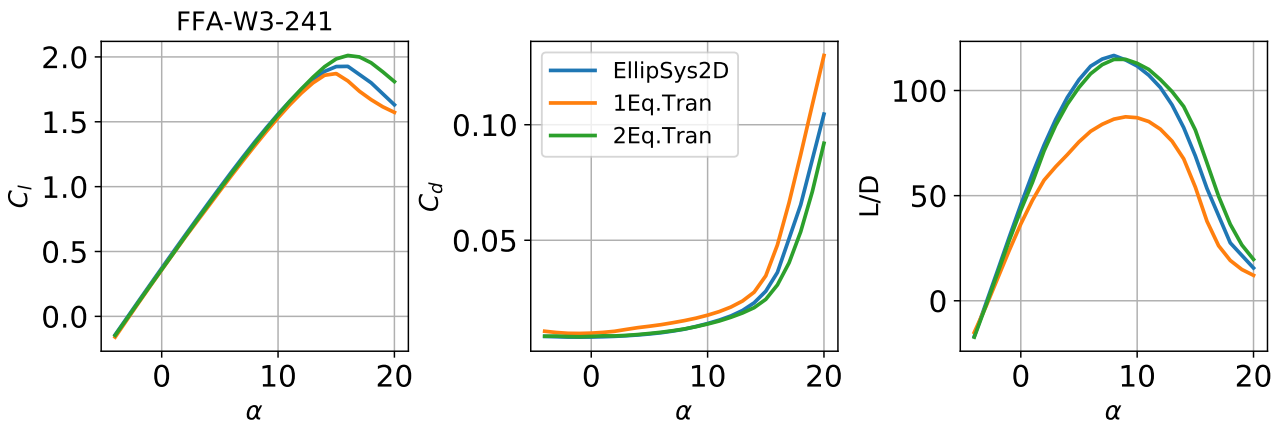
(Sec. 4.2). The differences between the predictions from the two transition models also increases with increase in thickness as observed earlier.

330 For a better understanding of the two-equation $\gamma - Re_{\theta t}$ model in HAM2D, we compare its behavior to the implementation of the same model (LCTM) in Ellipsys-2D using the $k-\omega$ -SST turbulence model for the FFA-W3-301 airfoil (Bak et al., 2013) at $Re = 10 \times 10^6$. The skin friction distribution predicted by HAM2D and Ellipsys-2D for this airfoil are compared at four different angles of attack in Fig. 12. The sign of skin friction is defined by the sign of the local streamwise velocity at each point. The transition onset location is indicated by a sharp increase in the skin friction value on both the upper and lower surfaces.

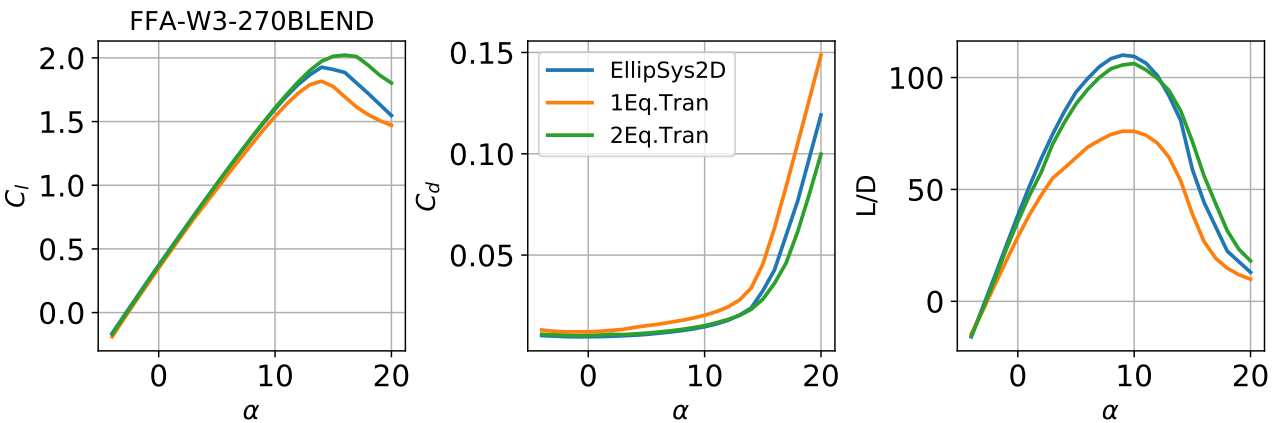
335 The transition onset prediction from the one-equation model in HAM2D rapidly moves to upstream at the 8° angle of attack. As a result, it predicts a delayed onset at the lower angles of attack, but earlier onset at the higher angles of attack compared against the EllipSys-2D result. On the other hand, the transition onset predicted by the two-equation model is downstream



(a) FFA-W3-211 airfoil at $Re = 10 \times 10^6$



(b) FFA-W3-241 airfoil at $Re = 10 \times 10^6$



(c) FFA-W3-270BLEND airfoil at $Re = 10 \times 10^6$

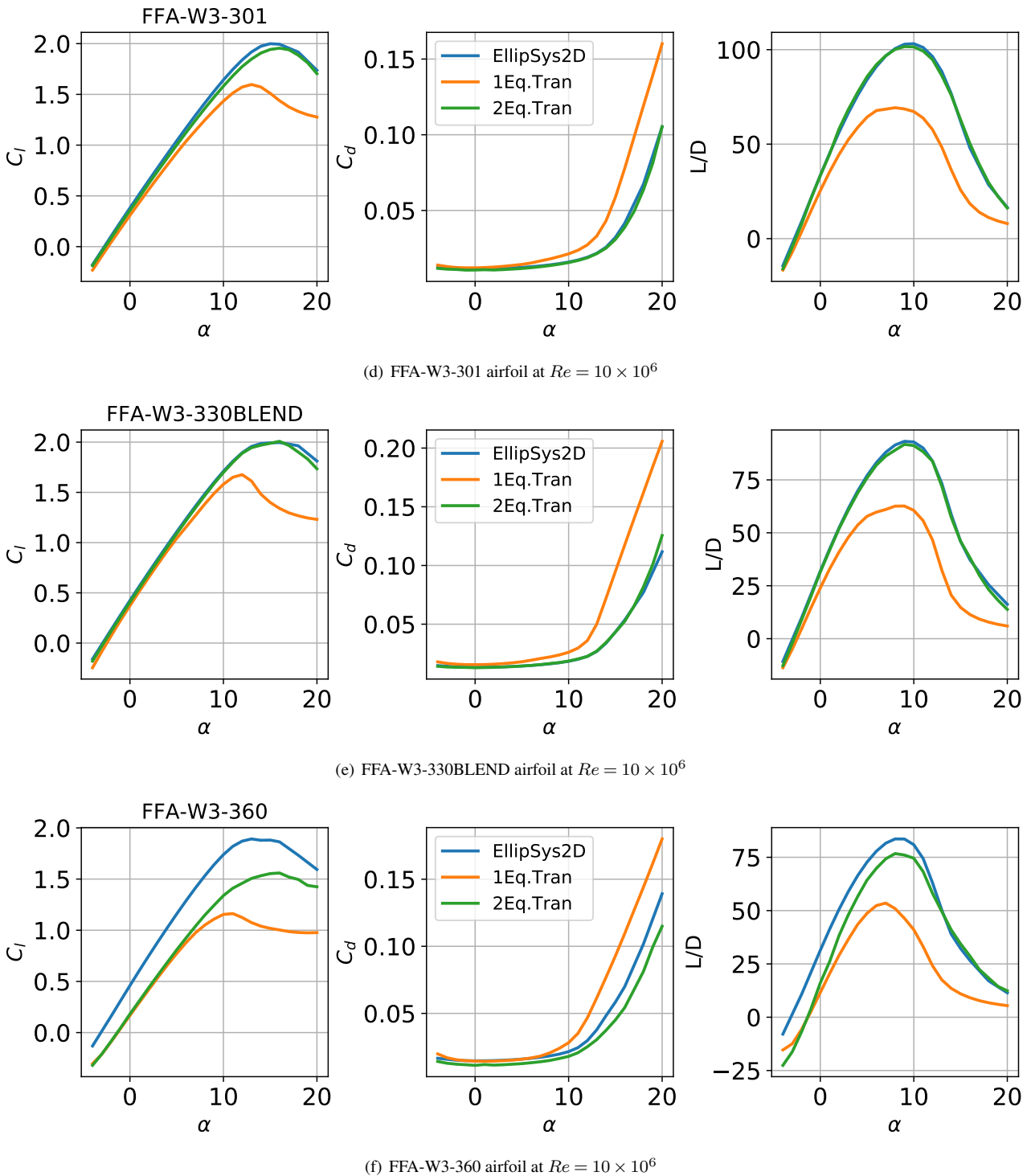


Figure 11. Aerodynamic coefficient polars for the FFA airfoil series using fully turbulent and free transition at $Re = 10 \times 10^6$ generated using HAM2D compared against a mix of 70%/30% transition/turbulent data from EllipSys-2D (Gaertner et al., 2020).

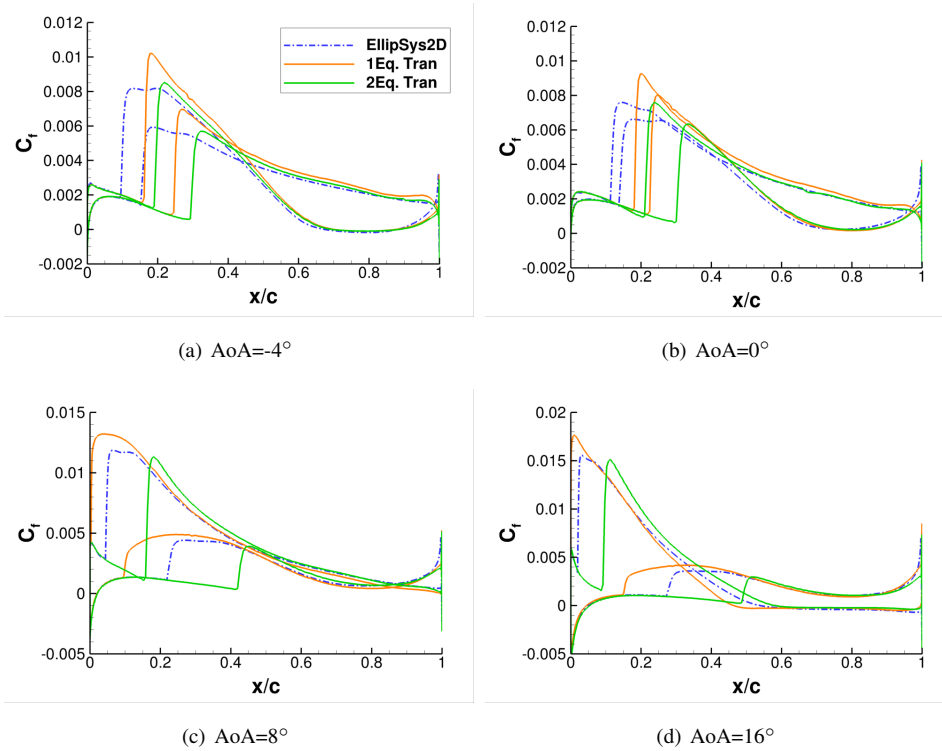


Figure 12. Skin friction coefficient distribution for the FFA-W3-301 airfoil at $Re = 10 \times 10^6$ generated using HAM2D with the one-equation and two-equation transition models compared against EllipSys-2D with the $\gamma - Re_\theta$ transition model (Bak et al., 2013).

of the predictions from the one-equation model and from EllipSys-2Da at all angles of attack. A similar behaviors was also observed for the DU-00-W212 airfoil at $Re = 9 \times 10^6$ in Fig. 8. This might be because the bypass transition effect is more accurately predicted by the two-equation model especially at the high Reynolds numbers. Thus, the two-equation model in HAM2D can capture the transition onset accurately, which results in the comparable airloads prediction with the e^N method, as shown in Fig. 11 (d).



5 Conclusions

We evaluated the performance of two local correlation-based transition models within our in-house 2D compressible Reynolds-averaged Navier-Stokes (RANS) solver HAM2D for applications to modern wind-turbine airfoils at high Reynolds numbers. The one-equation transition model (γ) and the two-equation transition model ($\gamma - \overline{Re_{\theta t}}$) are coupled with the Spalart-Allmaras (SA) one-equation turbulence model. We compare the predictions of the two transition models with available experimental and computational fluid dynamics (CFD) data in the literature in the Reynolds number range of 3-15 million including the AVATAR project measurements of the DU00-W-212 airfoil (Ceyhan et al., 2017a) and for airfoils from three modern, commercially relevant wind turbines, NREL 5 MW (Jonkman et al., 2009), DTU 10 MW (Bak et al., 2013), and IEA 15 MW (Gaertner et al., 2020).

The two models exhibit similar behavior at Reynolds numbers around 3 million. The one-equation transition model fails to predict the natural transition behavior at the high Reynolds numbers ranging from 6 million to 15 million due to early transition onset, as reported in previous studies (Sorensen et al., 2016). The two-equation transition model presents much better predictions in aerodynamic coefficients (e.g. stall angle, maximum lift coefficient, and lift-to-drag ratio) than the one-equation transition model. As a result, comparable performance with the e^N -based transition models within RANS-CFD are observed for the various thickness airfoils. The one-equation transition model also fails to predict the correct trends of the aerodynamic coefficients, especially the peak lift-to-drag ratio, with Reynolds number. On the other hand, the prediction of the trends in aerodynamics coefficients with Reynolds number from the two-equation transition model is much closer to that of the experimental data and comparable to the predictions from the e^N -based models in the literature (Ceyhan et al., 2017b). The predictions from the two-equation transition model exhibits a strong sensitivity to the free-stream turbulence intensity, as reported by Ceyhan et al. (2017b). A limitation of the two-equation model is observed at Reynolds numbers greater than 12 million, wherein the predictions are particularly sensitive to the inflow turbulent intensity. Overall, the combination of the ($\gamma - \overline{Re_{\theta t}}$) transition model coupled with the Spalart-Allmaras RANS turbulence model is a robust method for performance prediction of modern wind-turbine airfoils using CFD.

The shortcomings of the one-equation transition model at high Reynolds numbers have been identified by comparing against the two-equation transition model. However, the one-equation transition model is more desirable for general wind-turbine applications because the model formulation is Galilean invariant. In the future, we plan to improve the performance of the one-equation transition model using the Field-Inversion Machine-Learning approach.



370 Appendix A: Grid Convergence Study

A grid convergence study was conducted to measure the sensitivity of airfoil performance to grid resolution to validate the current grid resolution. The grid convergence study was performed for the airfoils using different number of surface points: 300, 400, 500, and 600. The initial wall normal spacing was fixed with a small enough value such that $y^+ = 1$. The test was focused at a specific operating flow condition with $\alpha=4^\circ$ and $Re = 9 \times 10^6$. The simulations are performed for both the fully turbulent and free-transition boundary layer. The results for the DU21 airfoil are shown in Figs. A1, A2, A3. The y-axis limit is the ranges of $\pm 1\%$ of each mean changes in the number of grid points. It is seen that the magnitude of the variation is less than 1% of their actual values, which results in minor variation compared to the variation from different airfoils or flow conditions of the current interest.

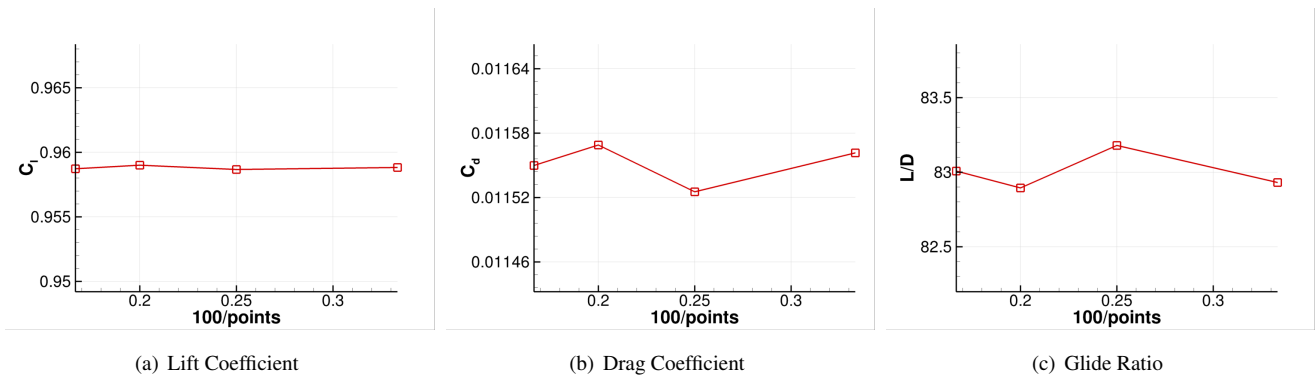


Figure A1. Grid resolution study for the DU21 airfoil at $\alpha=4^\circ$ and $Re=9M$ (fully turbulent flow)

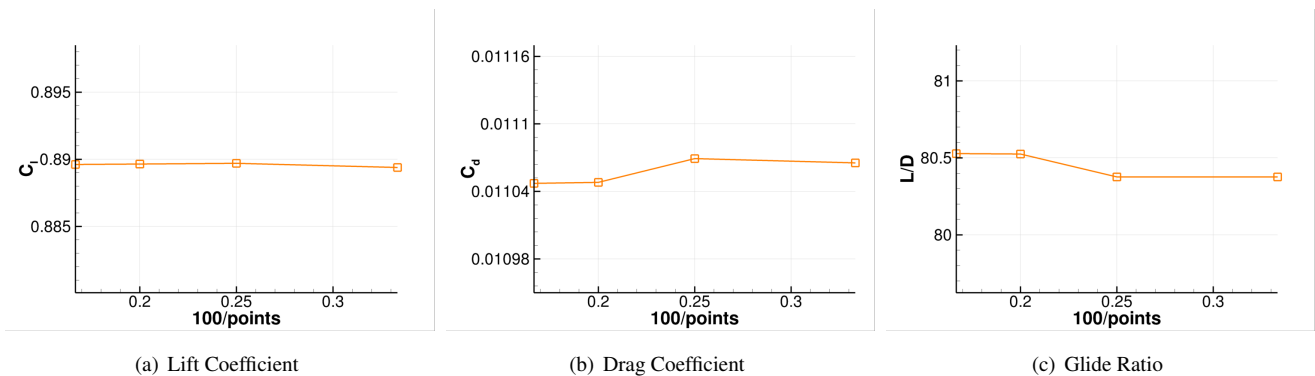


Figure A2. Grid resolution study for the DU21 airfoil at $\alpha=4^\circ$ and $Re=9M$ (free-transition using the one-equation model)

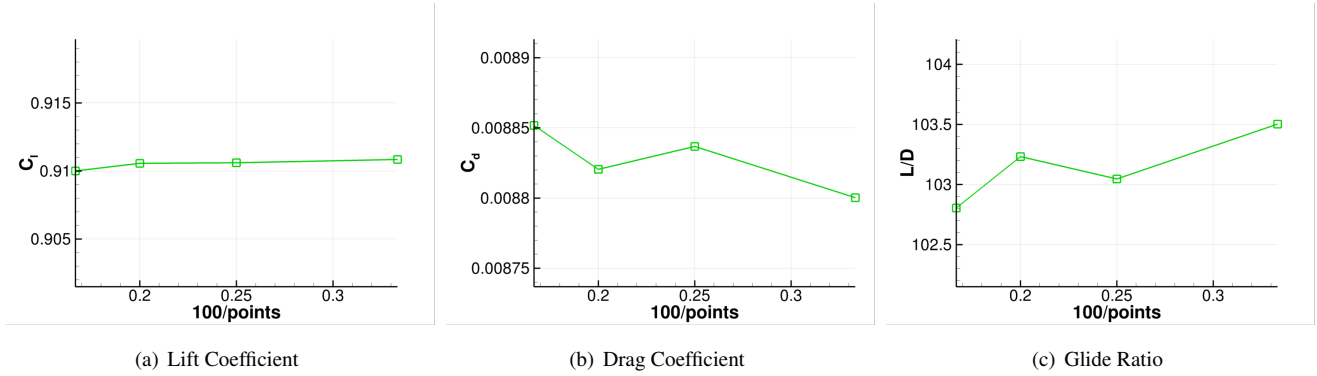


Figure A3. Grid resolution study for the DU21 airfoil at $\alpha=4^\circ$ and $Re=9M$ (free-transition using the two-equation model)

Appendix B: Solution Convergence Study

380 Figures B1 and B2 show the solution convergence history during the simulation for the representative flow condition at two different Reynolds numbers of 3×10^6 and 9×10^6 . Both lift and drag coefficients are converged within 1500 iterations, wherein the solution residual drops by more than 3 orders of magnitude.

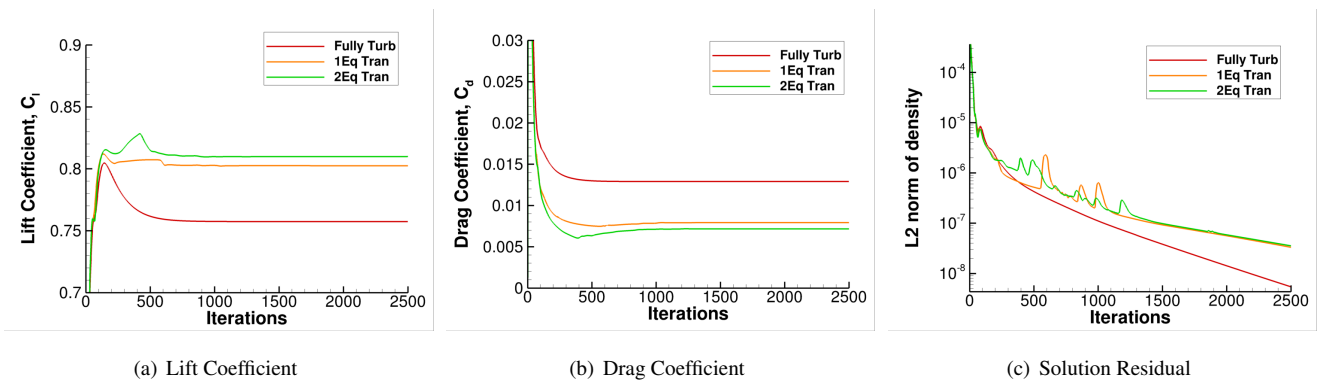


Figure B1. Solution convergence history during simulations for the DU-00-W212 airfoil at $\alpha=4^\circ$ and $Re=3M$

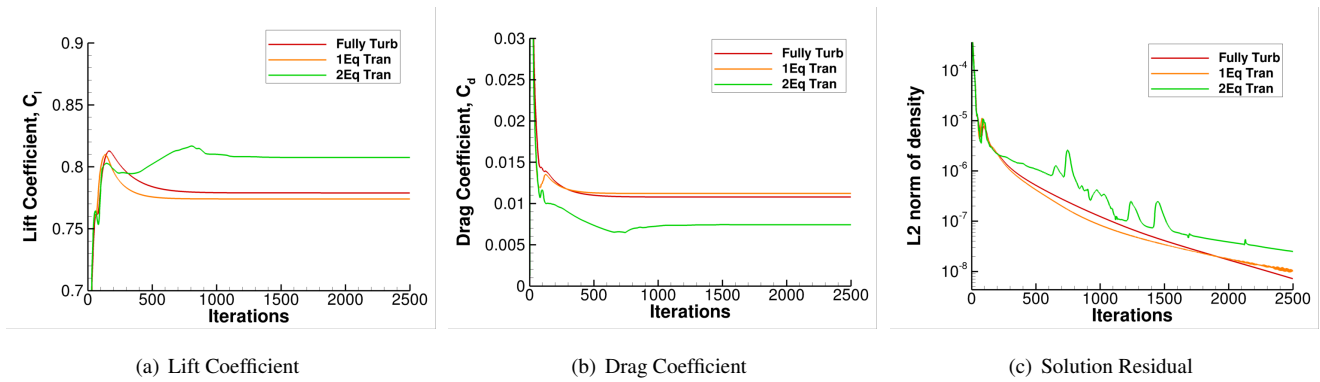


Figure B2. Solution convergence history during simulations for the DU-00-W212 airfoil at $\alpha=4^\circ$ and $Re=9M$



Data availability. Data for any plots in this manuscript can be made available on request

Author contributions. YSJ developed the simulation code and performed the simulations. YSJ wrote the manuscript with significant input
385 from GV. GV provided reference data set and developed the post-processing code for the simulation results. SA and JB provided guidance
for the research and reviewed the manuscript.

Competing interests. The authors declare that they have no conflict of interest.

Acknowledgements. This work was authored in part by the National Renewable Energy Laboratory, operated by Alliance for Sustainable
Energy, LLC, for the U.S. Department of Energy (DOE) under Contract No. DE-AC36-08GO28308. Funding provided by the Advanced
390 Research Projects Agency-Energy (ARPA-E) Design Intelligence Fostering Formidable Energy Reduction and Enabling Novel Totally Im-
pactful Advanced Technology Enhancements (DIFFERENTIATE) program. The views expressed in the article do not necessarily represent
the views of the DOE or the U.S. Government. The U.S. Government retains and the publisher, by accepting the article for publication, ac-
knowledges that the U.S. Government retains a nonexclusive, paid-up, irrevocable, worldwide license to publish or reproduce the published
form of this work, or allow others to do so, for U.S. Government purposes. A portion of this research was performed using computational
395 resources sponsored by the Department of Energy's Office of Energy Efficiency and Renewable Energy and located at the National Renew-
able Energy Laboratory. The transition modeling work was supported under the Vertical Lift Research Center of Excellence Grant at the
University of Maryland with Dr. Mahendra Bhagwat as Technical Mentor.



References

- Turbulence Modeling Resource, Tech. rep., NASA Langley Research Center, <http://turbmodels.larc.nasa.gov>, 2017.
- 400 AVATAR - Advanced aerodynamic modelling, design and testing for large rotor blades, Tech. rep., European Energy Research Alliance, 2018.
- Allmaras, S., Johnson, F., and Spalart, P.: Modifications and Clarifications for the Implementation of the Spalart-Allmaras Turbulence Model, in: ICCFD7-1902, 7th International Conference on Computational Fluid Dynamics, 2012.
- Bak, C., Zahle, C., Bitsche, R., Kim, T., Yde, A., Henrikson, L. C., Hansen, M. H., Blasques, J. P. A. A., Guanaa, M., and Natarajan, A.: The
405 DTU 10-MW Reference Wind Turbine, Tech. rep., DTU, <https://findit.dtu.dk/en/catalog/2389486991>, 2013.
- Ceyhan, O., Pires, O., and Munduate, X.: AVATAR HIGH REYNOLDS NUMBER TESTS ON AIRFOIL DU00-W-212 [Dataset], Tech. rep., <https://doi.org/http://doi.org/10.5281/zenodo.439827>, <https://windbench.net/avatar-2d-high-reynolds>, 2017a.
- Ceyhan, O., Pires, O., Munduate, X., Sorensen, N., Reichstein, T., Schaffarczyk, A., Diakakis, K., G, P., Daniele, E., M, S., Lutz, T., and
410 Prieto, R.: Summary of the Blind Test Campaign to predict the High Reynolds number performance of DU00-W-210 airfoil, in: AIAA Scitech, 2017b.
- Coder, J.: Further Development of the Amplification Factor Transport Transition Model for Aerodynamic Flows, in: AIAA Scitech, 2019.
- Colonia, S., Leble, V., Steijl, R., and Barakos, G.: Calibration of the γ -Equation Transition Model for High Reynolds Flows at Low Mach, Journal of Physics: Conference Series, 753, 2016.
- Costenoble, A., Govindarajan, B., Jung, Y., and Baeder, J.: Automated Mesh Generation and Solution Analysis of Arbitrary Airfoil Geome-
415 tries, in: AIAA Aviation, 2017.
- Costenoble, A., Jung, Y., Govindarajan, B., and Baeder, J.: Automated Mesh Generation and Solution Analysis of Arbitrary Airfoil Geome- tries, in: AHS Technical Conference on Aeromechanics Design for Transformative Vertical Flight, 2018.
- Drela, M. and Giles, M. B.: Viscous-Inviscid Analysis of Transonic and Low Reynolds Number Airfoils, AIAA Journal, 25, 1347–1355, 1987.
- 420 Gaertner, E., Rinker, J., Sethuraman, L., Zahle, F., Anderson, B., Barter, G., Abbas, N., Meng, F., Bortolotti, P., Skrzypinski, W., Scott, G., Feil, R., Bredmose, H., Dykes, K., Sheilds, M., Allen, C., and Viselli, A.: Definition of the IEA 15 MW Offshore Reference Wind Turbine, Tech. rep., International Energy Agency, <https://www.nrel.gov/docs/fy20osti/75698.pdf>, 2020.
- Hall, Z.: Assessment of Transition Modeling Capabilities in NASA’s OVERFLOW CFD Code version 2.2m, in: AIAA Scitech, 2018.
- Hand, M., Simms, D., Fingersh, L., Jager, D., Cotrell, J., Schreck, S., and Larwood, S.: Unsteady Aerodynamics Experiment Phase VI: Wind
425 Tunnel Test Configurations and Available Data Campaigns, Tech. rep., NREL/TP-500-29955, National Renewable Energy Laboratory, 2001.
- Jonkman, J., Butterfield, S., Musial, W., and Scott, G.: Definition of a 5-MW Reference Wind Turbine for Offshore System Development, Tech. Rep. NREL/TP-500-38060, NREL, Golden, CO, 2009.
- Jung, Y.: Hamiltonian Paths and Strands for Unified Grid Approach for Computing Aerodynamic Flows, Ph.D. thesis, University of Maryland, 430 2019.
- Jung, Y. S. and Baeder, J.: $\gamma - Re_{\theta_t}$ Spalart–Allmaras with Crossflow Transition Model Using Hamiltonian–Strand Approach, Journal of Aircraft, 56, 1040–1055, <https://doi.org/10.2514/1.C035149>, <https://doi.org/10.2514/1.C035149>, 2019.
- Jung, Y. S., Govindarajan, B., and Baeder, J.: Turbulent and Unsteady Flows on Unstructured Line-Based Hamiltonian Paths and Strand Grids, AIAA Journal, 55, 1986–2001, 2017.



- 435 Langtry, R. B. and Menter, F. R.: AIAA Journal, 47, 2894–2906, 2009.
- Lee, B. and Baeder, J.: Prediction and validation of laminar-turbulent transition using SA- γ , in: AIAA Scitech, 2021.
- Medida, S.: Correlation-based Transition Modeling for External Aerodynamic Flows, University of Maryland PhD Dissertation, 2014.
- Menter, F., Smirnov, P., Liu, T., and Avancha, R.: A One-Equation Local Correlation-Based Transition Model, Flow Turbulence Combust., 95, 583–619, 2015.
- 440 Nichols, R.: Addition of a Local Correlation-Based Boundary Layer Transition model to the CREATE-AV Kestrel Unstructured Flow Solver, in: AIAA Scitech, 2019.
- Pires, O., Munduate, X., Ceyhan, O., Jacobs, M., and Snel, H.: Analysis of high Reynolds numbers effects on a wind turbine airfoil using 2D wind tunnel test data, Journal of Physics: Conference Series, 753, 2016.
- Sheng, C.: Advances in Transition Flow Modeling: Applications to Helicopter Rotors, Springer Nature, 2017.
- 445 Somers, D. M.: Design and Experimental Results for the S809 Airfoil, Tech. rep., NREL/SR-440-6918, National Renewable Energy Laboratory, 1997.
- Sorensen, N., Zahle, F., and J., M.: Prediction of airfoil performance at high Reynolds numbers, in: EFMC2014, 2014.
- Sorensen, N., Mendez, B., Munoz, A., Sieros, G., E., J., Lutz, T., Papadakis, G., Voutsinas, S., Barakos, G., Colonia, S., Baldacchino, D., Baptista, C., and Ferreira, C.: CFD code comparison for 2D airfoil flows, Journal of Physics, 753, 2016.
- 450 Veers, P., Dykes, K., Lantz, E., Barth, S., Bottasso, C. L., Carlson, O., Clifton, A., Green, J., Green, P., Holttinen, H., Laird, D., Lehtomäki, V., Lundquist, J. K., Manwell, J., Marquis, M., Meneveau, C., Moriarty, P., Munduate, X., Muskulus, M., Naughton, J., Pao, L., Paquette, J., Peinke, J., Robertson, A., Sanz Rodrigo, J., Sempreviva, A. M., Smith, J. C., Tuohy, A., and Wisser, R.: Grand challenges in the science of wind energy, Science, 366, <https://doi.org/10.1126/science.aau2027>, <https://science.sciencemag.org/content/366/6464/eaau2027>, 2019.
- Wang, J. and Sheng, C.: Validation of a local correlation-based transition model using an unstructured CFD solver, in: AIAA Theoretical Fluid Mechanics Conference, 2014.
- 455 Yilmaz, O.: Summary of the Blind Test Campaign to predict the High Reynolds number performance of DU00-W-210 airfoil, in: AIAA Scitech, 2017.